TUS

JOURNAL OF GEOPHYSICAL RESEARCH, VOL. 105, NO. D14, PAGES 18,067–18,089, JULY 27, 2000

Preliminary estimation of horizontal fluxes of cloud liquid water in relation to subtropical moisture budget studies employing ISCCP, SSMI, and GEOS-1/DAS data sets

Yuval Shay-El and Pinhas Alpert

Department of Geophysics and Planetary Sciences, Tel Aviv University, Israel

Arlindo da Silva

Data Assimilation Office, NASA Goddard Space Flight Center, Greenbelt, Maryland

Abstract. Special Sensor Microwave/Imager (SSM/I) retrievals of cloud liquid water, International Satellite Cloud Climatology Project (ISCCP) cloud estimates, and winds from the Goddard EOS (GEOS-1/DAS) assimilation are employed to evaluate vertically integrated cloud liquid water (CLW) transport for 1992. First, GEOS-1/DAS multiyear data are used to confirm an earlier finding of a paradoxical net moisture sink over the Arabian-Iraqi desert [*Alpert and Shay-El*, 1993]. The negative vertically integrated moisture flux divergence over this region is balanced mainly by the negative incremental analysis updates (IAU) of moisture. Moisture fluxes reveal strong convection but without precipitation in a shallow Hadley-type cell. Vertical profiles indicate that the moisture removal process is associated with middle and high clouds and probably with CLW flux divergence. The CLW fluxes are estimated explicitly and globally from ISCCP and SSM/I by using linear regression methods. Areas of significant CLW divergence are found over the eastern coasts of both the United States and Asia, in the vicinity of the Gulf Stream and Kuroshio currents, as earlier conjectured by *Peixoto* [1973]. In both the Arabian-Iraqi desert and over the Sahara, divergence of a vertically integrated CLW flux opposes the convergence of a vertically integrated horizontal moisture flux, thus explaining at least partially the paradoxical net sink and source in these regions. However, the magnitude of the annual CLW flux estimates as calculated here is, in general, too small to play any significant role in the vertically integrated water budget, except perhaps along coastal regions and over dry subtropical deserts where precipitation minus evaporation is relatively small.

1. Introduction

This article is dedicated to the late great worldwide scholar Jose Pinto Peixoto who passed away on December, 6, 1996, at the age of 74. P. Alpert was honored to have discussions with him while delivering a seminar in the Geophysical Fluid Dynamics Laboratory (GFDL) on this paper's topic on March 18, 1996, following an invitation by A. Oort. The study was much stimulated also by earlier attempts of *Peixoto* [1973] to evaluate the importance of the cloud liquid water (CLW) fluxes in moisture budget studies.

In climate studies of moisture budgets the horizontal transport of condensed water is usually neglected. This is often justified by the smaller value of the horizontal transport of cloud liquid water (CLW) compared to the horizontal transport of water vapor. *Peixoto and Oort* [1992, p. 275] mention a possible exception to this rule being the case of dense cumulonimbus clouds in the tropics or over ocean currents, as suggested by *Peixoto* [1973]. Thus the vertically integrated moisture equation is commonly simplified to a balance between the time-averaged divergence of the vertically integrated moisture vapor flux in an atmospheric column ($\mathbf{Q}$) and the averaged evaporation (E) minus precipitation (P), or

$$\nabla \cdot \overline{\mathbf{Q}} = \overline{E} - \overline{P} \tag{1}$$

when the storage term can be neglected. The overbar denotes time averaging, and $\mathbf{Q}$ is defined by

$$\mathbf{Q} = \int_{p_t}^{p_s} \mathbf{V} q \mathrm{d}p/g \tag{2}$$

Paper number 1999JD901200.
0148-0227/00/1999JD901200$09.00

where $\mathbf{V}$ is the horizontal wind vector, q is the specific humidity, g is the gravity constant, p_s is the surface pressure, and p_t is the top pressure.

There are relatively large regions, however, where this balance seems to be violated. In particular, if the horizontal fluxes of cloud liquid water are not negligible, then equation (1) should include another term, i.e., $\nabla \cdot \overline{\mathbf{Q}}_c$, where $\mathbf{Q}_c$ is the vertically integrated cloud liquid water flux, to read:

$$\nabla \cdot \overline{\mathbf{Q}} + \nabla \cdot \overline{\mathbf{Q}}_c = \overline{E} - \overline{P}. \quad (3)$$

It is the main purpose of this study to estimate the commonly neglected horizontal fluxes of cloud liquid water.

The original motivation for this study is the finding of a net moisture sink or negative $\nabla \cdot \overline{\mathbf{Q}}$ over the Arabia-Iraqi desert during winter. This feature was first noted by *Alpert and Shay-El* [1993] (hereinafter referred to as AS) who used 6 years of operational European Centre for Medium-Range Weather Forecasts (ECMWF) analyses and is depicted in Figure 1a, following AS. It is also prominent in the more recent NASA Goddard EOS data assimilation system (GEOS-1/DAS) data set [*Schubert et al.*, 1993], as shown in Figure 1b. Since this desert region has very scarce rainfall (Figure 1c), the excess of rainfall over evaporation as a possible explanation can be easily ruled out. The probable scenario suggested by AS is that cloud condensation exceeds evaporation but is not compensated by rainfall at the surface. Frequent medium- and high-level clouds, which develop in this region, are horizontally advected out of the region by the prevailing subtropical jet, removing in the form of cloud droplets the water vapor which converged to this region. This scenario will be reexamined in section 2, based on GEOS-1/DAS. In section 3 we will present first explicit global estimates of cloud liquid water divergence which will be used for further study of this region in section 4.1. A similar although inverse question relates to the net moisture source over the Sahara as mentioned by *Starr and Peixoto* [1958] and studied recently by *Shay-El et al.* [1999]. The potential of cloud liquid water advection in explaining this unusual finding will also be addressed briefly in section 4.2.

It must be emphasized that equation (1) does not strictly hold when the fields $\mathbf{Q}$, E, and P come from a data assimilation system [e.g., *Schubert et al.*, 1995, p. 69]. The correct moisture budget equation in this case reads

$$\nabla \cdot \overline{\mathbf{Q}} = \overline{E} - \overline{P} + \Delta + < \text{filter} >, \quad (4)$$

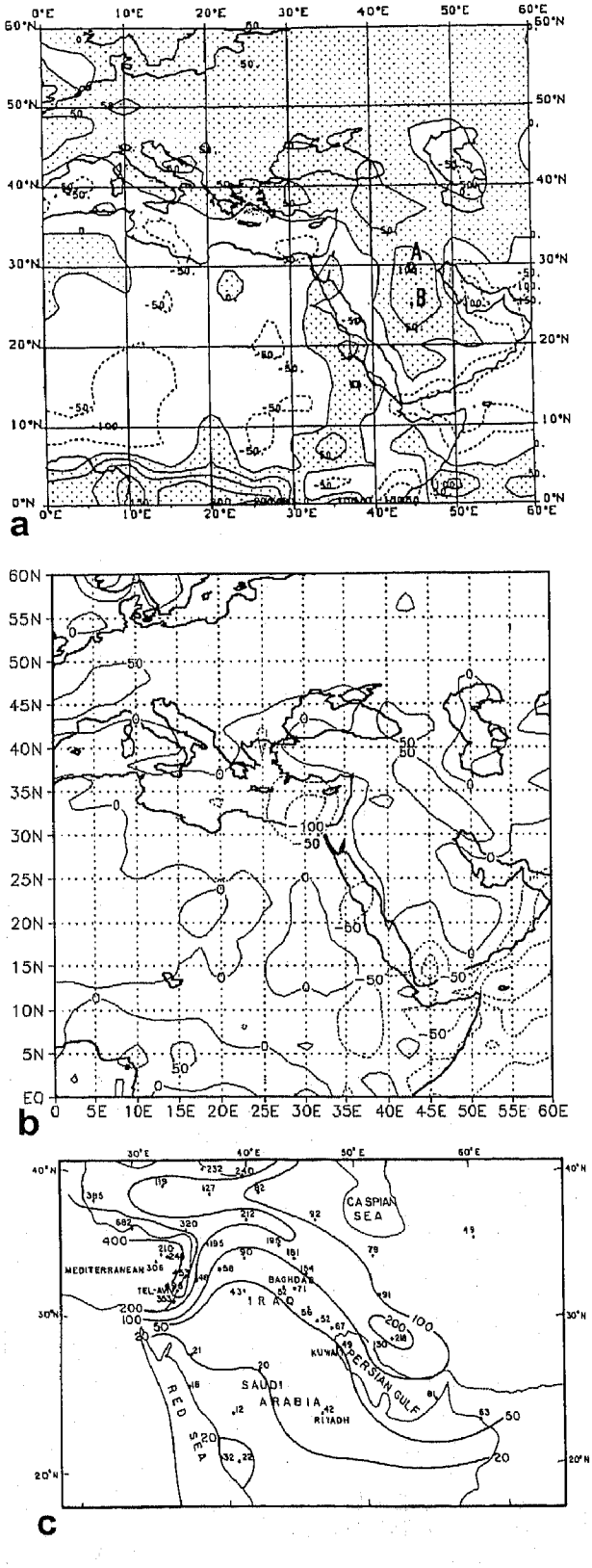

Figure 1. Mean terms of the vertically integrated moisture balance, for winter (December-February): (a) Moisture flux convergence, i.e., $-\nabla \cdot \mathbf{Q}$, calculated from ECMWF 1982-1988 operational analysis data, following *Alpert and Shay-El* [1993, Figure 2, p. 191]. Positive (solid) and negative (dashed) contours are in intervals of 50 W m^{-2}. Positive value regions are shaded. Points A and B for later reference in Figures 6 and 7. (b) Same as Figure 1a but from NASA GEOS-1/DAS 1985-1993 reanalysis data. (c) Rainfall distribution, following *Alpert and Shay-El* [1993, Figure 1, p. 191]. Contour levels are 20, 50, 100, 200, 400 mm (equivalent to 6, 16, 32, 64, and 128 W m^{-2}).

where Δ, which is proportional to the mean vertically integrated incremental analysis updates for specific humidity, or IAU(q), represents the correction of the model state by the observational data; and the vertically integrated <filter> includes the effects of the Shapiro smoothing filter and any filling of moisture to remove negative specific humidity. The Δ term compensates for biases in the estimates of $\nabla \cdot \overline{\mathbf{Q}}$, $\overline{E}$, and $\overline{P}$, or any physical process not represented in the atmospheric general circulation model used in the assimilation system, such as the CLW. In a region with adequate data coverage the mean analysis increments can provide a useful diagnostic tool. The role of the analysis increments in the Saudi-Iraqi desert will be discussed in section 2.

The three-dimensional moisture balance, without vertical integration, will be employed as well. The form of the equation to be used is

$$\frac{\partial \overline{q}}{\partial t} = -\nabla \cdot \overline{q\mathbf{V}} - \frac{\partial \overline{q\omega}}{\partial p} + \overline{S}_q, \qquad (5)$$

where we will assume that the annual mean storage (i.e., $\partial \overline{q}/\partial t$ on the left-hand side of equation (5)) is negligible (see, for example, AS). The term S_q is the net moisture source, calculated as follows:

$$S_q = \frac{\partial q}{\partial t}_{\text{moist}} + \frac{\partial q}{\partial t}_{\text{turb}} + \frac{\partial q}{\partial t}_{\text{IAU}} + \frac{\partial q}{\partial t}_{\text{filter/filling}}, \qquad (6)$$

where $\partial q/\partial t_{\text{moist}}$ (or moist$Q$ hereinafter) is the specific humidity changes due to moist parameterizations of convective processes and of large-scale precipitation processes, or supersaturation rain, $\partial q/\partial t_{\text{turb}}$ (or turb$Q$) is due to turbulence, $\partial q/\partial t_{\text{IAU}}$ (or IAU(q)) is due to the analysis increments, and $\partial q/\partial t_{\text{filter/filling}}$ (or filter) is due to the smoothing filter and the filling of moisture to remove negative specific humidity. The vertical integration of turb$Q$ and moist$Q$ result in the evaporation (E) and the precipitation ($-P$), respectively. The model parameterizations being used in GEOS-1/DAS are described by *Takacs et al.* [1994].

The method applied here for explicit estimates of CLW fluxes makes use of vertically integrated, monthly mean cloud liquid water retrievals over the global oceans from the Special Sensor Microwave/Imager (SSM/I) [*Wentz*, 1995]. These retrievals are extended over the continents by regressing cloud information from the International Satellite Cloud Climatology Project (ISCCP) [*Rossow and Schiffer*, 1991]; details of the method are given in section 3. Global monthly mean estimates of CLW are combined with winds from the GEOS-1/DAS to provide estimates of the monthly mean cloud liquid water divergence. Reassessments of both the Arabian net sink paradox and the Sahara net source are performed in section 4 with the aid of the newly derived estimates for CLW and $\nabla \cdot$ CLW fields, and discussion and conclusions are presented in section 5. It must be emphasized that the estimation of CLW over land is very preliminary. The regression methodology described in section 3 is intended as an extended "back of the envelope" calculation which attempts to express cloud fluxes in units of cloud liquid water fluxes. The limitations and potential shortcomings of this approach are discussed in sections 3 and 5.

2. Eight-Year Annual Mean Moisture Balance Over the Saudi-Iraqi Desert

2.1. NASA GEOS-1/DAS Data Set

The GEOS-1/DAS reanalysis data set, used extensively in this work, is produced by the Data Assimilation Office of the NASA Goddard Space Flight Center [*Schubert et al.*, 1993]. Parallel reanalysis efforts are being conducted at the National Centers for Environmental Prediction (NCEP) [*Kalnay et al.*, 1996] and at the European Centre for Medium-Range Weather Forecasts (ECMWF) [*Gibson et al.*, 1994]. Besides eliminating spurious climatic signals arising from changes in the operational analysis system, reanalysis products include a wealth of diagnostic quantities which historically have not been made available with the operational products. Of particular interest for moisture budget studies and atmosphere/surface interactions are the estimates of moisture transports, precipitation, evaporation and clouds, along with several boundary layer and convective diagnostic quantities.

In this study we use 8 years of available data, from March 1985 to February 1993. In a related paper, *Shay-El et al.* [1999] have employed the same set of data for studying the moisture budget over the Sahara desert along with the involved uncertainties. *Schubert et al.* [1998] have also employed the same set of data for examining variations in the moisture entering the continental United States from the Gulf of Mexico, with a particular emphasis on the role of low-level southerly jets and the impact of continental warm-season precipitation. *Min and Schubert* [1997a, b] compared the NASA reanalysis with the NCEP reanalysis and ECMWF operational analyzed data set in relation also to regional moisture studies. They summarize that on average, the reanalysis products show higher coherence with each other than with the operational product in the estimates of interannual variability of moisture fluxes.

2.2. Vertically Integrated Balance

Figures 1a and 1b compare the vertically integrated moisture flux convergence term ($-\nabla \cdot \mathbf{Q}$, neglecting the overbar for simplicity) over the Middle East for an average winter (December-February) from the operational ECMWF analysis, with that from the GEOS-1/DAS reanalysis. It should be noted that the mean ECMWF convergence was calculated off line, using snapshots of the wind and humidity every 12 hours on seven pressure levels. On the other hand, the mean GEOS-1/DAS con-

vergence, as well as the other budget terms discussed later, were summed up every time step on the model sigma levels and are included among other mean diagnostic outputs of the assimilation system. Only the spatial derivatives (i.e., ∇ and $\partial/\partial p$ operators) were calculated off line with the grids analysis and display system (i.e., GrADS) [e.g., *Doty*, 1995].

The convergence term in Figure 1 is given in units of latent heating rate (W m^{-2}), following the earlier AS study. According to equation (1) it should balance the $P - E$ term; therefore it is sometimes called the apparent net moisture sink. For comparison, Figure 1c shows the precipitation distribution calculated only from local observations in millimeter units (1 mm is equivalent to 0.32 W m^{-2} for this time period), following AS. The contours of $-\nabla \cdot \mathbf{Q}$ in Figure 1b seem to closely follow the precipitation contours in Figure 1c along the high-topography region stretching to the northwest from the Persian Gulf. The ECMWF analysis (Figure 1a), however, does not reveal this feature, but a maximum of ~100 W m^{-2} over the very dry Arabian desert to the west of the Persian Gulf (point A in Figure 1a). In comparison, GEOS-1/DAS (Figure 1b) produces over this region much smaller values of ~30 W m^{-2} (equivalent to ~95 mm for the 3 month period). Nevertheless, these values are still higher compared to the observations in Figure 1c; hence although NASA reanalysis seems more realistic than the operational ECMWF, the "paradox" of a net moisture sink is still apparent. For further reassessment of this paradox, a detailed examination of the other moisture balance terms, and the evaporation in particular, follows.

Figure 2 shows the 8 year annual mean terms of the vertically integrated moisture balance (equation (4)) using the NASA GEOS-1/DAS data set averaged for March 1985 to February 1993 and focusing over the Arabian peninsula. All units are in millimeter per day, and negative values are shaded. $\nabla \cdot \mathbf{Q}$, E, and P are shown in Figures 2a, 2b, and 2c. The diagnostic E and P fields are produced by the model parameterizations with only an indirect impact by observations. The difference field, $E - P$, the increments field IAU(q), and the filter term are shown in Figures 2c, 2d, and 2e. The filter term was estimated as a residual of the other terms following, for example, *Schubert et al.* [1995, p. 69]. The fact that $\nabla \cdot \mathbf{Q}$ (Figure 2a) and $E - P$ (Figure 2d) have different signs confirms the hypothesis of an apparent net moisture sink over most of the Arabian peninsula.

Unlike the earlier AS study, GEOS-1/DAS enables us to distinguish among the components of the apparent moisture sink; thus it can provide more information on the origin of this sink. In particular, it is important to note that $\nabla \cdot \mathbf{Q}$ is negative due to the increments IAU(q) and not due to the parameterized $E - P$. This means that the negative divergence is not a model artifact, because the model parameterizations really "pull" in the other direction, toward a source (similarly to other subtropical deserts such as the Sahara desert [*Shay-El et al.*, 1999]); and it is only due to the observation corrections, i.e., IAU(q), that the final assimilated divergence is negative. *Trenberth and Guillemot* [1998] also noted this feature over Saudi Arabia, based on NCEP reanalysis. They associated it with excessive evaporation in their model. This explanation might be partly applicable here as well. Nevertheless, it is important to notice that the resulting negative $\nabla \cdot \mathbf{Q}$ (Figure 2a) is even greater than the precipitation P (Figure 2c). This means that even if we would have assumed a zero evaporation, there still would have been left an unexplained residual divergence.

The filter (Figure 2e) mainly smoothes the water/land boundary and pumps water vapor into land from the surrounding water bodies which have prominent evaporation (see Figure 2b). *Shay-El et al.* [1999] suggested that this numerical diffusion may partly correspond to real physical diffusion mechanisms such as sea breeze advection which is a subgrid scale phenomenon not realistically reproduced by the synoptic scale assimilation system.

2.3. Moisture Flux Fields

In Figure 3 the upper panel shows the 8 year annual mean moisture transport vectors and divergence over the Arabian Peninsula region for the vertically integrated flux and for the 900 hPa and 700 hPa isobaric levels, from GEOS-1/DAS. In the bottom panels of the figure, the fluxes are depicted as streamlines. The vertically integrated streamlines (Figure 3d) reveal an anticyclonic subtropical cell over the Arabian desert, with pronounced fluxes from the Mediterranean associated with the aforementioned convergence over the peninsula (Figure 3a). This vertically integrated picture does not show the drastic changes with height. The boundary layer moisture streamlines at 900 hPa (Figure 3e) enter Arabia from all directions, resulting in strong low-level convergence (Figure 3b), in particular over the southern, more elevated, tip of the peninsula. At 700 hPa (Figure 2c), however, these convergence zones turn out to be divergence zones, reflecting strong and mostly dry convection over this region.

This convection is further illustrated in the vertical cross section of the moisture flux streamlines along 45°E (Figure 4). A Hadley-type cell can be seen, with the ascending branch above the elevated topography at the south of the Arabian Peninsula (14°N–20°N). This vertical circulation is also linked with strong subtropical westerlies as evident from the uq core (dark shadings) at 700 hPa level and 28°N latitude. The vertical cell is quite distinct, in comparison, for example, with a more typical Hadley cell circulation over Africa (e.g., AS, Figure 4a, not shown here) in the sense that the convection at the ascending branch is not associated with heavy tropical precipitation but with almost no precipitation at all (Figure 2c). It is also more shallow, and the center of the vortex is slightly above ground level at 950 hPa (27°N latitude), whereas over Africa, it was found

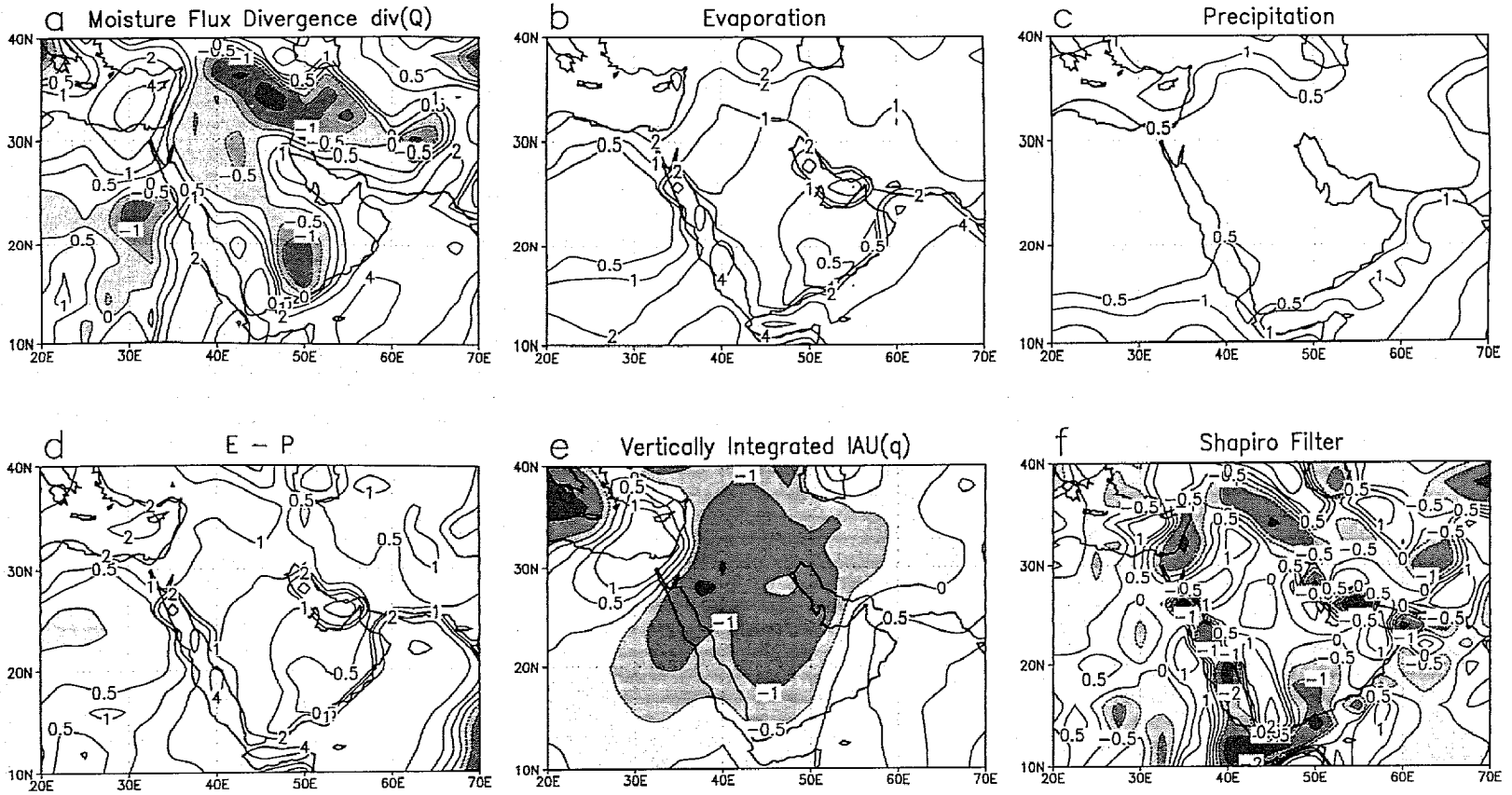

Figure 2. Eight year annual mean components of the vertically integrated moisture balance, calculated from the NASA GEOS-1/DAS data set, averaged from March 1985 to February 1993 over the Arabian Peninsula. Top panel shows moisture flux divergence $\nabla \cdot \mathbf{Q}$ (a), evaporation (b), and precipitation (c); bottom panel shows (d) evaporation minus precipitation, $E - P$, (d), the incremental analysis updates for the specific humidity, IAU(q), (e), and the filter (f). All units are millimeter per day. Contour levels are $0, \pm 0.5, \pm 1, \pm 2, \pm 4, \pm 6, \pm 8, \pm 10$ mm/d. Negative values are shaded.

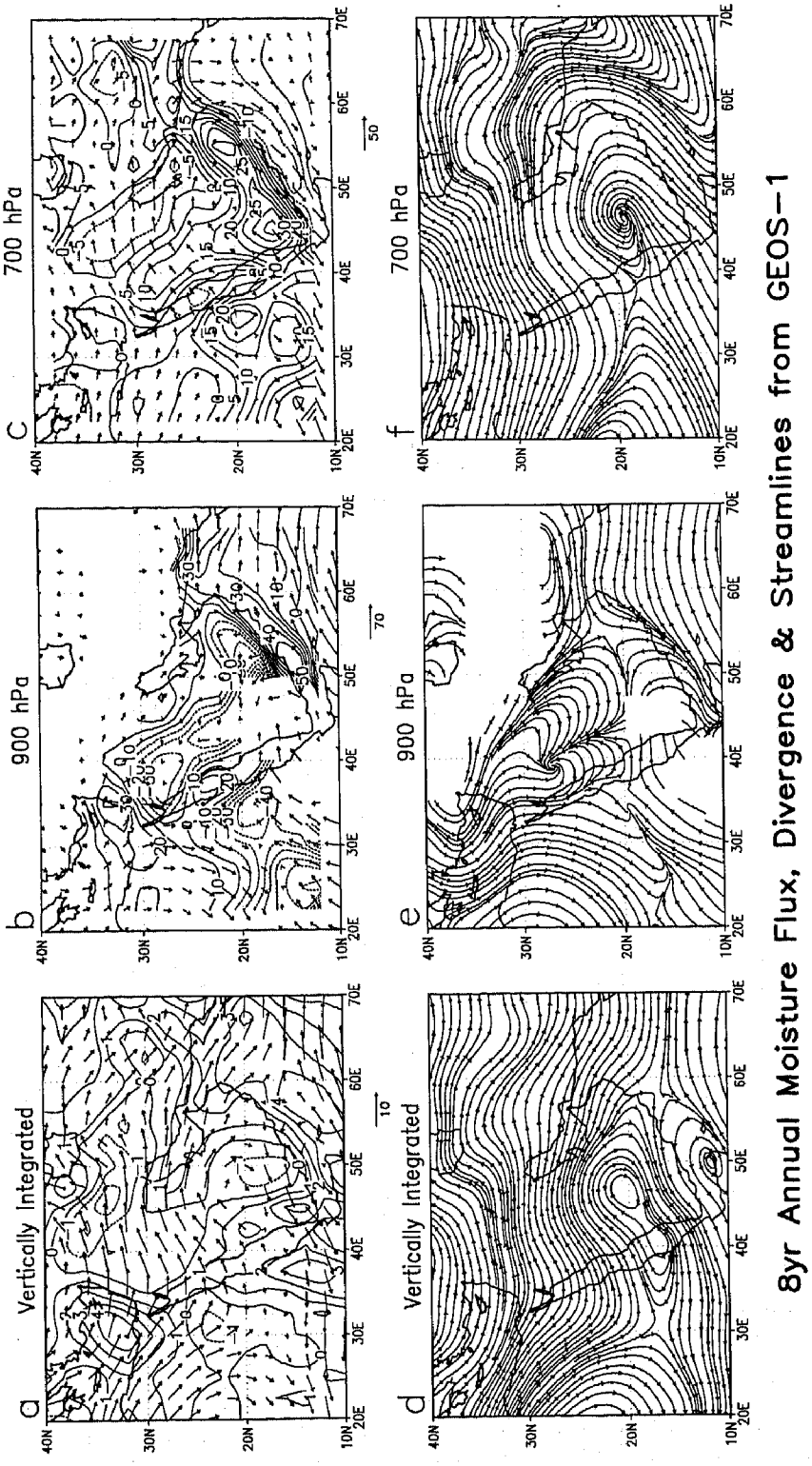

Figure 3. Eight year annual mean moisture transport fields, calculated from the NASA GEOS-1/DAS data set: (a) Vertically integrated moisture flux vectors, in units m/s g/kg, and divergence contours (mm/d); (b) same as Figure 3a but for the 900 hPa level and divergence units of 10^{-6} g kg^{-1} s^{-1}; (c) same as Figure 3b but for the 700 hPa level. Below are the corresponding horizontal streamlines for (d) the vertically integrated moisture flux, (e) the 900 hPa level, and (f) the 700 hPa.

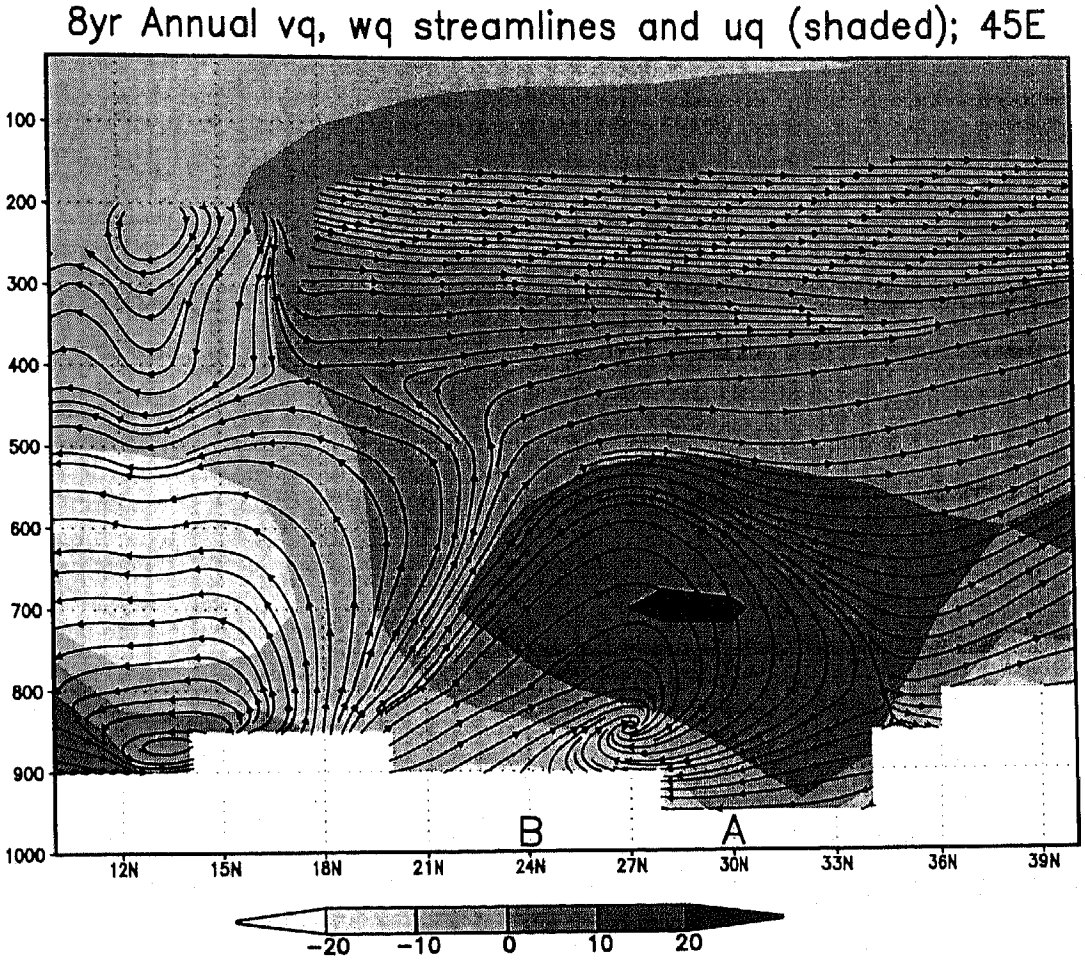

Figure 4. Vertical cross section of the 8 year annual mean moisture flux streamlines $(vq, \omega q)$ along longitude 45°E, and uq in shadings, calculated from the NASA GEOS-1/DAS data set. A shading bar, in units of 10^{-6} g kg^{-1} m s^{-1}, is at the bottom of the figure. Points A and B for later reference are in Figures 6 and 7.

at 700 hPa (24°N latitude, AS, Figure 4a). This particular circulation may be associated with medium cloud activity, such as evaporating rain, and will be discussed in section 2.4.

2.4. Vertical Cross Sections and Profiles

Figure 5 shows the vertical cross section of the annual mean moisture incremental analysis updates, i.e., IAU(q), along 45°E, with sigma as the vertical coordinate. For the corresponding pressure levels, see caption. The increments are negative over most of the cross section (north of 15°N), which means that the IAU(q) act to remove excessive moisture in the model first guess. Most important to note is that over most of the Arabian Peninsula (south of 30°N) the maximum of IAU(q) is well off ground, at sigma level 0.75, equivalent to ~690 hPa. This supports the AS hypothesis that this moisture-removing process might be associated with CLW advection in particular in middle-level cloudiness. Large negative values of up to -11×10^{-6} g kg^{-1} s^{-1} near the surface are found over the Zagros Mountains at 36°N. These might be associated with the maximal moisture convergence band over this mountainous region (e.g., Figure 2a).

The role of clouds and the link of the microphysical processes with the dynamics are more evident from the profiles of the terms of the three-dimensional moisture balance (equation (5)). Figures 6a and 6b depict these profiles for two selected grid points A and B at 45°E, 30°N and 45°E, 24°N. These two points noted on Figure 1a were studied also by AS (i.e., AS, Figures 6-8, not shown here). (In AS, point B was at latitude 25°N and not 24°N because of a different grid resolution.) The line with long dashes in each of these figures is the horizontal moisture convergence, or minus divergence $(-\nabla \cdot \overline{q}\overline{\mathbf{V}})$; i.e., positive values act to increase the moisture content, and its vertically integrated value is $-\nabla \cdot \mathbf{Q}$. Similarly, the line with short dashes is the vertical convergence $(-\partial \overline{q\omega}/\partial p)$, calculated from the assimilated vertical moisture flux on pressure levels. Its vertically integrated value should therefore be zero, and deviations from zero are only due to numerical errors in

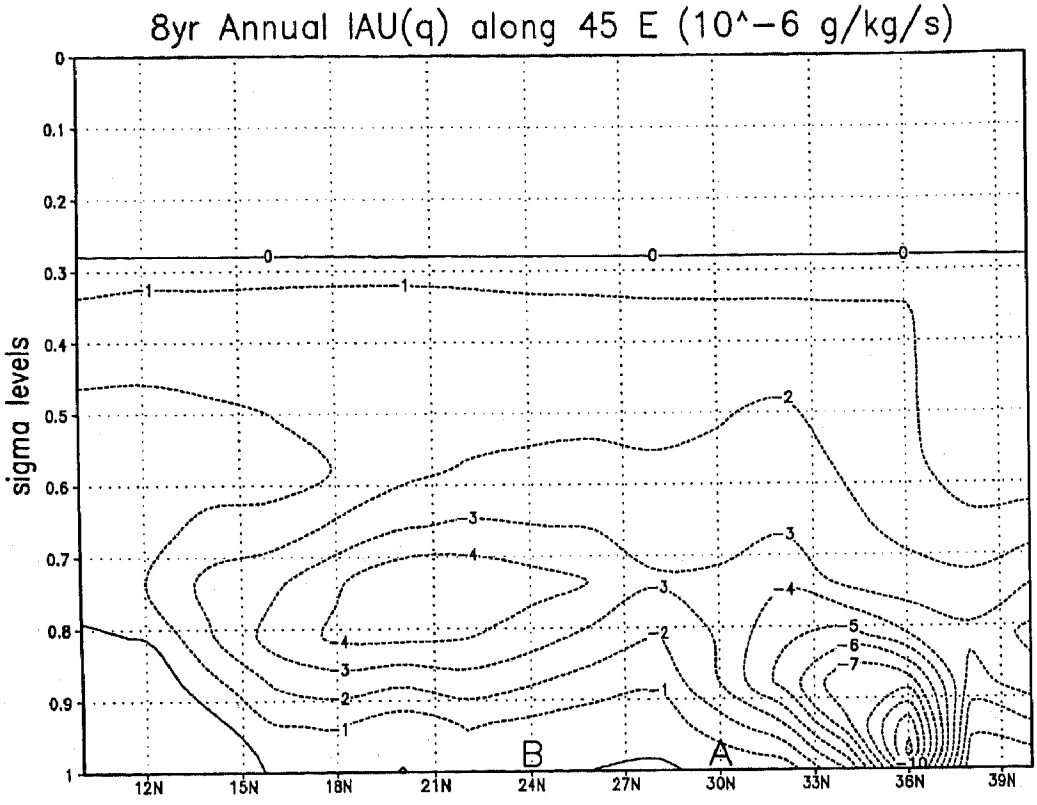

Figure 5. Vertical cross section of the annual mean IAU(q) along 45°E, in units of 10^{-6} g kg^{-1} s^{-1}, with sigma levels for vertical coordinate. Sigma levels 1, 0.8, 0.6, 0.4, 0.2, 0 approximately correspond to pressure levels of 920, 740, 550, 370, 190, and 10 hPa. Points A and B for later reference are in Figures 6 and 7.

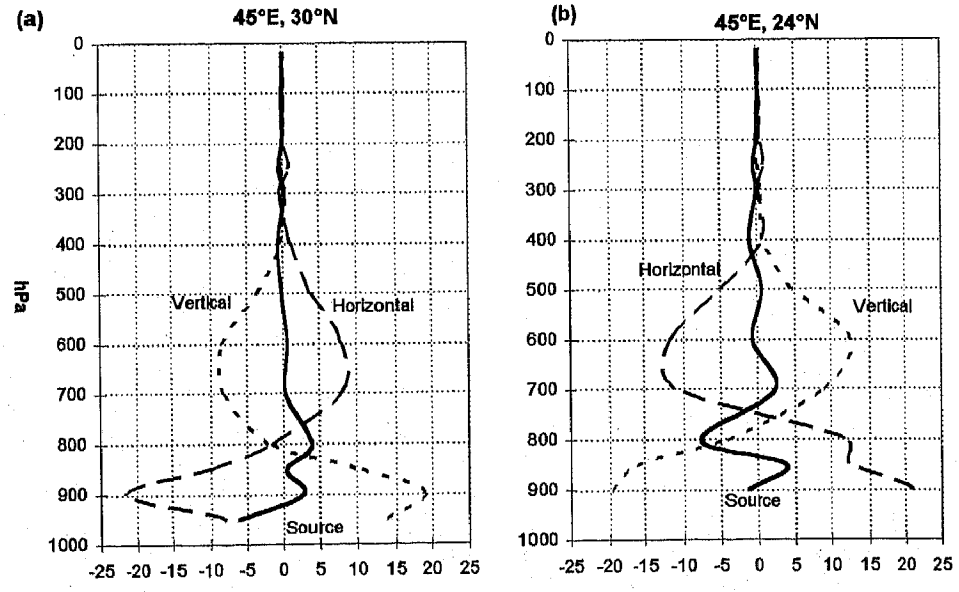

Figure 6. (a, b) Vertical profiles of the terms of the three-dimensional moisture balance, equation (5), for the NASA 8-year annual means, at point 45°E, 30°N (point A in Figure 1a), and 45°E, 24°N (point B), respectively. Horizontal convergence line is long dashed, vertical convergence is short dashed, and the apparent net source, calculated as residual, is solid. All values are in 10^{-6} g kg^{-1} s^{-1} units.

the calculation on pressure levels and not on the sigma levels of the model. The solid line is the apparent moisture net source S_q, calculated as the residual in the moisture equation. For annual means the storage can be neglected [AS; *Shay-El et al.*, 1999]; hence the three lines sum to zero at each isobaric level.

In both Figures 6a-6b the dynamical terms are more prominent compared with the residual source. Point A is in the descending branch of the Hadley-type cell mentioned above (Figure 4). As might be expected from this, moisture converges at levels above 800 hPa, is removed to lower levels by subsidence, and then diverges (Figure 6a). Point B, even if only three grid points apart, is in the ascending branch. Consequently, the relation between the vertical component and the horizontal one is just the opposite, with convergence in low levels, transport to upper levels by the ascending motion, and divergence in the upper levels. In the AS study, based on ECMWF data, vertical motion was less prominent, and the balance was primarily between the net sink and the horizontal moisture convergence. These differences might be partly due to the use of the advection form of the moisture balance equation in AS, and not the flux form, and also because in AS, points A and B were in the middle of the region with maximum negative $\nabla \cdot \mathbf{Q}$, whereas here they are almost on the "zero" contour of the vertically integrated divergence (Figure 2a).

It should be emphasized that S_q includes not only the subgrid and physical moisture processes but also the incremental analysis updates IAU(q), which correct for errors in these processes and in the dynamical transport terms, and also the filter term. The GEOS-1/DAS data set provides also the diagnostic fields of the moisture change due to turbulence (turb$Q$) and due to moist processes (moist$Q$). These profiles, the IAU(q) term, and the filter term are shown in Figures 7a-7b for the A and B grid points, respectively. The filter was estimated as the residual from the other terms and the S_q. The vertical integration of turb$Q$ and moist$Q$ result in the evaporation (E) and the precipitation ($-P$), respectively.

In both Figures 7a-7b, turb$Q$ moistens the air up to high levels, as high as 500 hPa in point B (Figure 7b), in accord with a convective circulation. Interestingly, moist$Q$ also has positive values, at levels below 800 hPa, indicating evaporation of falling convective raindrops. The GEOS-1/DAS model has a parameterization for this process which is described by *Sud and Molod* [1988]. This significant middle-cloud activity was also supported by synoptic reports (AS). The IAU(q) term removes moisture all along the columns, with peaks at ~700 hPa. This seems to be linked with cloud activity and possibly with CLW divergence. One might speculate that the increments correct for errors in the parameterizations of turb$Q$ and moist$Q$, but this would have resulted in excessive precipitation which does not correspond to the observations. Therefore it is plausible that this correction is associated with an absent nonprecipitating cloud process, such as CLW advection.

Finally, the filter, as mentioned before, not only consists of the horizontal Shapiro filter but also of the filling of moisture from below to remove negative specific humidity. The latter process might be the reason for the "noisy" structure of the filter profile. It is also interesting to note that in spite of the great differences in the dynamical terms of the moisture balance between points

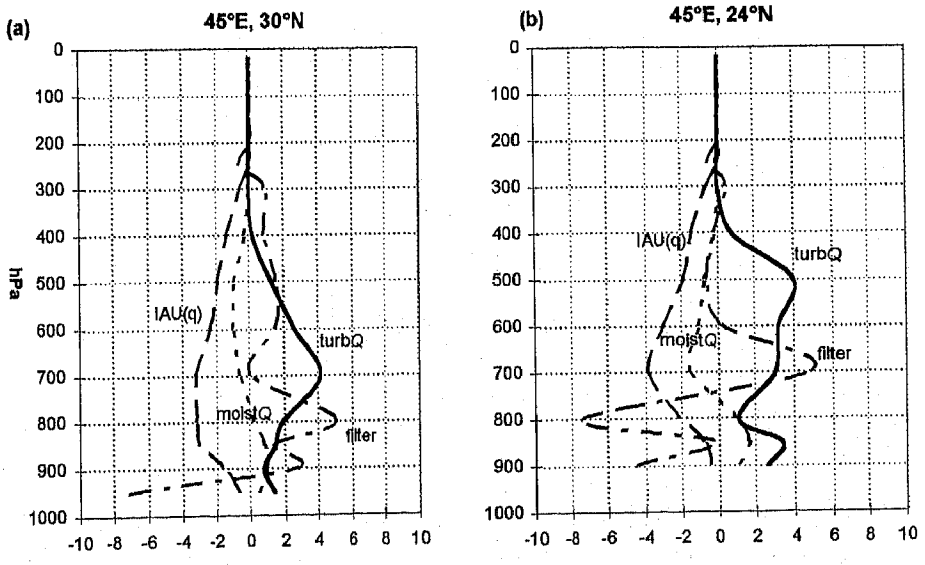

Figure 7. (a, b) Same as Figures 6a and 6b but for the moisture changes due to turbulence (turb$Q$, solid line), moist processes (moist$Q$, short dashed), increments (IAU(q), long dashed), and the filter (long-short dashed). Notice the different abscissa scales compared with Figure 6. All values are in 10^{-6} g kg^{-1} s^{-1} units.

A and B (Figures 6a-6b) the subgrid-scale terms (Figures 7a-7b) are quite similar. This might be related to the large-scale character of the middle and high clouds.

3. Estimation of CLW Fluxes from SSM/I, ISCCP, and GEOS-1 Fields

3.1. Data and Methodology

The recent advent of well-calibrated satellite microwave radiometers enable the depiction of long time series of atmospheric water phases, including cloud liquid water (CLW). In this study we use 12 monthly means for 1992 of the CLW retrievals by *Wentz* [1995]. These retrievals are based on measurements of the SSM/I on the DMSP satellites. The retrieval algorithm is based on a radiative transfer model for the brightness temperature of the ocean and the intervening atmosphere. The retrieved parameters are the near-surface wind speed, the column-integrated water vapor, the column-integrated cloud liquid water, and the line-of-sight wind.

Cloud water values are available both for no rain and rainy cases. *Wentz* [1995] estimates the cloud liquid water root-mean-square (RMS) accuracy at about 2.5 mg cm^{-2} (or 0.025 mm) for a space resolution of 50 km. Typical values of CLW for nonrain clouds range from 0.05 to 0.20 mm and greater. When there is rain, the accuracy of the model is much degraded because the partitioning of cloud water and rainwater is not unique. Therefore the model is restricted to ocean scenes free of rain, and when the algorithm detects rain, the retrievals are discarded. Other methods for retrieving CLW from SSM/I data are proposed by *Greenwald et al.* [1995] and *Ferraro et al.* [1996]. We have binned the original CLW retrievals (at the satellite footprint) on a 2° latitude by 2.5° longitude grid with a 6 hour window, and subsequently, these 6 hour means were averaged to form monthly means and then the annual mean for 1992. No other smoothing has been applied. This CLW data set cannot be used directly for the Arabian Peninsula moisture study because it is restricted to ocean scenes. Nevertheless, cloud amounts are available from the International Satellite Cloud Climatology Project (ISCCP) [*Rossow and Schiffer,* 1991]. The oceanic cloud amounts are used here to obtain a linear relationship between the CLW from SSM/I and the ISCCP cloud amounts. The regression coefficients are later used to scale the cloud amounts over land to CLW units, thus providing some estimate for the CLW content over the continental regions as well. For this study we use the ISCCP D2 cloud data set [*Rossow et al.,* 1996]. The data for the 1992 monthly means were downloaded from the Internet (http:/isccp.giss.nasa.gov/browsed2.html).

The ISCCP analysis combines satellite-measured with the TIROS Operational Vertical Sounder (TOVS) atmospheric temperature-humidity (TV data) and ice/snow (IS data) correlative data sets to obtain information about clouds and the surface. The analysis method first determines the presence or absence of clouds in each individual image pixel and retrieves the radiometric properties of the cloud for each cloudy pixel and of the surface for each clear pixel. The pixel analysis is performed separately for each satellite radiance data set and the results are reported in the Stage DX data product, which has a nominal resolution of 30 km and 3 hours. The Stage D1 product is produced by summarizing the pixel-level results every 3 hours on an equal-area map grid with 280 km resolution and merging the results from separate satellites with the TV and IS data sets to produce global coverage at each time. The Stage D2 data product is produced by averaging the Stage D1 data over each month, first in each of the eight 3 hour time intervals individually and then over all eight time intervals. The first version of ISCCP cloud products, the C series, covered the period from July 1983 to June 1991. Further details about the changes between the C series and the improved D series are in the work of *Rossow et al.* [1996].

One of the important assumptions of ISCCP is that all image pixels containing clouds are completely covered by a single, homogeneous layer. The cloud detection procedure decides whether each satellite pixel is cloudy or clear. Total cloudiness is calculated in the D1 set by the fraction of the number of cloudy pixels and the total number of pixels. From the IR analysis, three cloud types are defined by the range of the cloud top pressure (PC): low (PC > 680 hPa), middle (680 < PC < 440 hPa), and high (PC < 440 hPa). In daytime these three cloud types are further divided into nine categories, defined by three cloud optical thickness intervals calculated from the visible radiance. In the D2 data set, D1 cloud amounts and other properties are averaged over the month. Here we employed the total cloudiness as well as the low-, middle-, and high-level cloudiness amounts, as described next.

For the calculation of the correlation between the SSM/I CLW and the ISCCP cloudiness we use two methods. Prior to the calculations, all data are interpolated to the GEOS 2° latitude by 2.5° longitude grid. In method **A** we calculate the relationship between the CLW and the total cloudiness using a linear regression, allowing the coefficients to vary by latitude (ϕ) and month. Thus the correlation is calculated from the longitudinal variability of the fields. The resulting prediction formula is

$$w = a_\phi \cdot c_{\text{tot}} + b_\phi, \tag{7}$$

where w is the CLW content, c_{tot} the fractional total cloud cover, and a and b the slope and intercept regression coefficients, respectively. This method allows us to investigate the variability of the correlation with respect to season and latitude. Correlations are examined not only for total cloudiness but also for low-, middle-, and high-level cloudiness.

The multiplicity of coefficients due to their variability with month and latitude enables good agreement (expressed by the coefficient of determination R^2) over

the ocean; however, it might reduce the robustness over land. Therefore in method **B** we use only three global coefficients, but unlike method **A**, we use a multiple linear regression function with the three cloud types as predictors; that is,

$$w = \alpha \cdot c_{\text{low}} + \beta \cdot c_{\text{mid}} + \gamma \cdot c_{\text{high}}, \quad (8)$$

where c_{low}, c_{mid}, and c_{high} are the low-, middle-, and high-cloud amounts, respectively, and α, β, and γ are their regression coefficients, respectively. This method allows the distribution of CLW among the three cloud types, and also the interpretation can be facilitated, since these CLW estimations are basically ISCCP cloud amounts multiplied by scaling constants.

Monthly mean winds from GEOS-1/DAS are used to calculate the CLW fluxes and their divergence. For the total CLW predicted in method **A** we use the 500 hPa winds. In method **B** we use the winds at sigma levels 0.8741, 0.7345, and 0.5005 for the low, middle, and high constituents, respectively. These sigma levels approximately correspond to ~870, 730, and 500 hPa pressure levels, respectively, with the advantage over the pressure levels of following the topography.

Some limitations of the approach just described should be outlined a priori. First, the total cloudiness reflect different types of clouds with significant differences in the CLW content. Some remedy for this shortcoming was achieved in method **B** by regressing CLW with the three types of clouds, i.e., low, medium and high, but still there is some mix between deep convection high clouds and cirrus, for example. Another related limitation is the fact that ice particles are not resolved by the SSM/I algorithm, while in ISCCP, ice clouds are an important component of the cloudiness. A third problem is that the CLW algorithm is restricted to no-rain conditions. These problems might reduce the correlation over ocean, and some consequences will be discussed later.

Another concern is that the regression relations over ocean may not be the same as over land. In fact, some variations certainly do exist since continental clouds differ from oceanic clouds [e.g., *Rossow and Schiffer*, 1991]. Finally, the use of monthly means for winds and cloudiness, while neglecting the wind-clouds covariance, might effect the mean CLW flux divergence. For a preliminary evaluation of this effect we have calculated the divergence of total cloudiness fluxes based on 6 hour winds and cloudiness from GEOS-1/DAS, and compared them to values obtained instead employing the monthly means. Not surprisingly, the eddy transport was found to be small in the tropics and subtropics, but of a magnitude comparable to the monthly mean transport in midlatitudes, particularly in the vicinity of the oceanic storm tracks. Although the CLW transport could have been calculated at the satellite footprint using the GEOS-1/DAS winds valid for each time, this was not yet done in the present preliminary study because our primary focus was on the subtropics and the associated paradoxes over the Arabian Peninsula and the Sahara.

3.2. Correlations Between SSM/I CLW and ISCCP Cloudiness

The 1992 annual mean of ISCCP total, low-, middle-, and high-level cloud amounts are shown in Figures 8a-8d, respectively. The total cloudiness (Figure 8a) is quite close to previous ISCCP statistics. *Rossow and Schiffer* [1991] associated regions with large cloud amounts with (1) the midlatitude ocean storm tracks, (2) the Intertropical Convergence Zone (ITCZ), and (3) off the west coasts of the continents in the subtropics. The first two types of regions are also noted in the middle-level and high-level cloudiness distributions (Figures 8c, 8d, respectively). The third type, associated with the marine stratus regimes, is reflected more by the low-level cloudiness distribution (Figure 8b), in particular off the west coasts of Africa and South America.

The predominance of stratus clouds in the low-level cloudiness distribution is due to the fact that ISCCP clouds are defined by the cloud-top pressure. This procedure is different than the classical one used for surface observations, where cloud level is defined by the cloud base. Consequently, deep convection clouds with high liquid water concentrations are associated with ISCCP high-level clouds, whereas classically deep convection clouds are associated with low-level clouds. *Rossow et al.* [1993] have also noted the smaller ISCCP cloud amounts than surface observations for low-level clouds and larger ISCCP cloud amounts than surface observations for high-level clouds.

Figure 9 shows the 1992 annual mean of SSM/I CLW in mg cm^{-2} (equivalent to 10^{-2} mm). As explained, CLW retrievals are available only over the ocean. Because of ice contamination the SSM/I retrievals of CLW are noisy and unreliable for latitudes higher than about 60°. The annual distribution shows high similarity with the total ISCCP cloudiness (Figure 8a). This similarity suggests that calculation of correlation between ISCCP clouds and SSM/I CLW over ocean may be useful for estimation of CLW amounts over land where retrievals are not available, employing ISCCP cloudiness over land.

Figures 10a-10d show the correlation coefficients (R) between monthly mean ISCCP clouds and SSM/I CLW for the total, low-, middle-, and high-level cloudiness, respectively. The correlations with the total cloud amounts are greater and more homogeneous in time and latitude than with the various level clouds. Not surprisingly, correlations are low at higher latitudes and not credible beyond 55° – 60° where both SSM/I and ISCCP have severe deficiencies.

In general, the correlation with high-level clouds (Figure 10d) is better than with middle-level or low-level clouds (Figures 10c, 10b). The latter shows the greatest seasonal and spatial variability, with even some negative correlations in particular over the midlatitudes and the

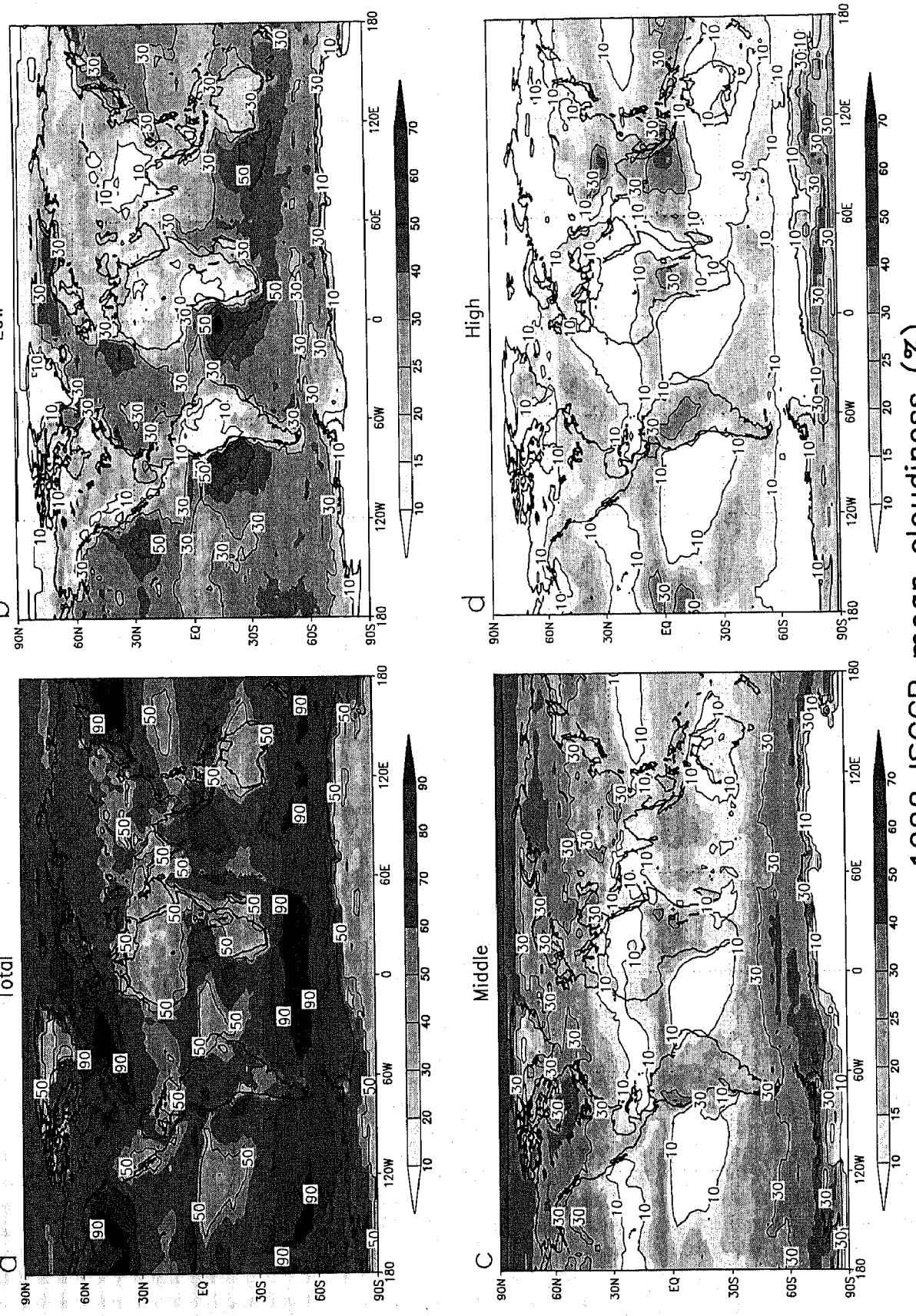

Figure 8. (a-d) 1992 annual means of ISCCP total, low-, middle-, and high-level cloud amounts (%).

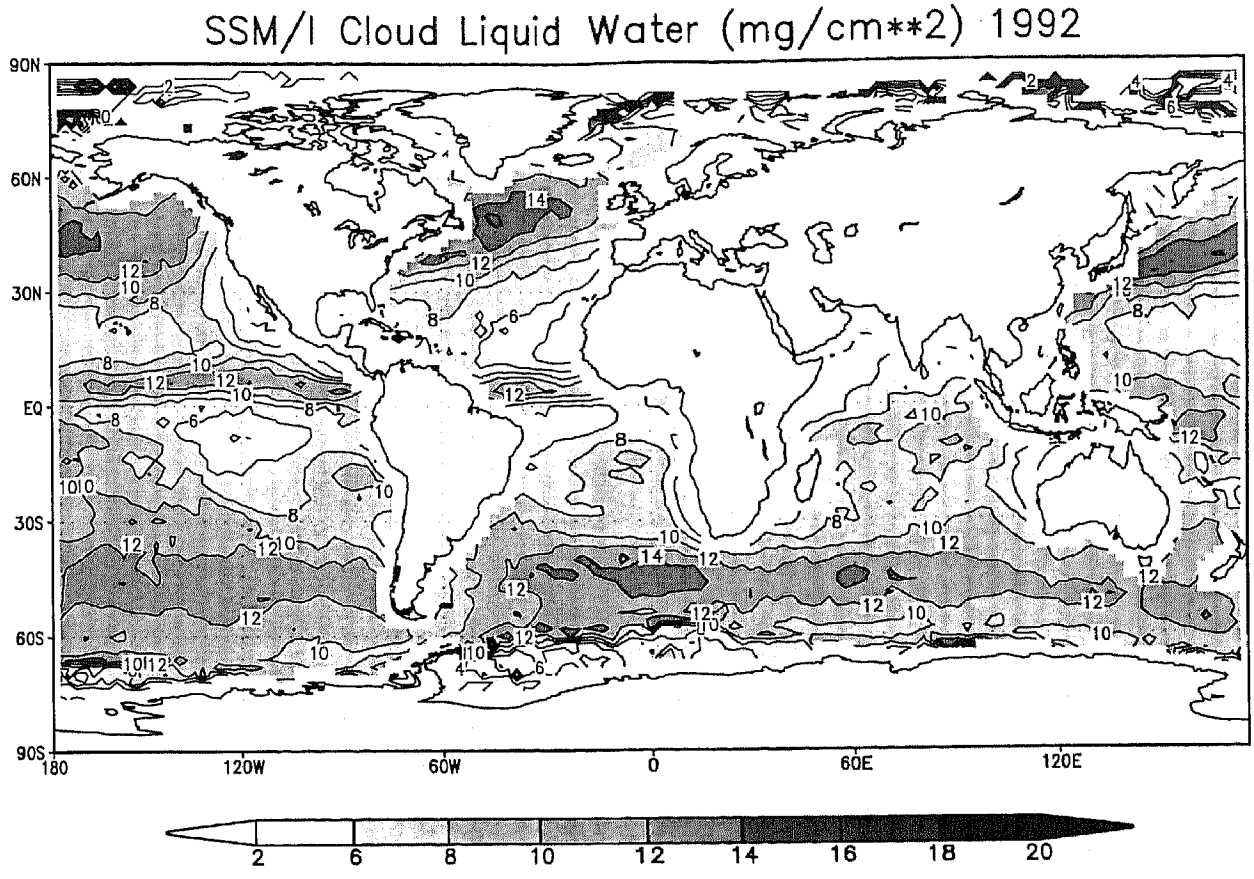

Figure 9. Cloud liquid water (CLW) from SSM/I in mg cm^{-2} (equivalent to 10^{-2} mm) for 1992, calculated from retrievals by *Wentz* [1995].

ITCZ. These anticorrelations must be associated with the anticorrelation between the low-level clouds and the high-level clouds, where low-level amounts are greater over the eastern oceanic regions (off the west coast of the continents), whereas high-level amounts are greater over the western oceanic regions and along the ITCZ, as seen in Figure 8. The correlation with the low-level clouds is high and positive only over the subtropics in summer with values as high as 0.7-0.8. These latter high correlations are also pronounced in the total cloudiness (Figure 8a). The total cloudiness has both the advantage of large correlations with the high-level and middle-level clouds over the midlatitude ocean storm tracks and the ITCZ and with the low-level clouds in the subtropics. It is therefore more suitable than the low-, middle-, or high-level cloudiness for prediction of CLW using equation (7). Correlations as small as 0.2 are found at the $10° - 20°$N latitude due to the greater longitudinal variability in the sharp transition between the ITCZ and the subtropics as evident in the CLW data (Figure 9), whereas the ISCCP cloudiness is much smoother (Figure 8a).

3.3. Estimation of CLW over Continents

We will now investigate the estimated vertically integrated CLW over the continents resulting from the correlation between the CLW from SSM/I and the total ISCCP cloudiness over the ocean, i.e., equation (7) (method **A**). A 5 point smoother, with weights of 0.083, 0.25, and 0.333 at the central point, was applied to the latitudinal variability of the coefficients a (slope) and b (intercept) in order to homogenize the horizontal scales present in the two data sets. Regressed negative CLW values are set to zero. The average values of a and b over time and latitude are 0.137 and -0.005 mm, respectively (where the cloudiness c is expressed as a fraction between zero and 1, and the resulting CLW content w is in millimeter units). The coefficient of determination R^2 for 1992 was calculated as the ratio of the predicted w sum of squares to the observed w sum of squares over the ocean, yielding 0.5844.

Plate 1a shows the resulting 1992 annual mean CLW global distribution in mg cm^{-2} (or 10^{-2} mm) along with the 500 hPa wind averaged for 1992. The winds are from the GEOS-1/DAS and were employed to calculate the monthly mean divergence of CLW. A comparison with Figure 9 reveals that the annual mean CLW distribution over ocean was largely conserved under the regression operator, as might be expected. Results over continents, however, can only be compared with model results. For example, there is high similarity with the annual mean CLW distribution derived by *Hack* [1998,

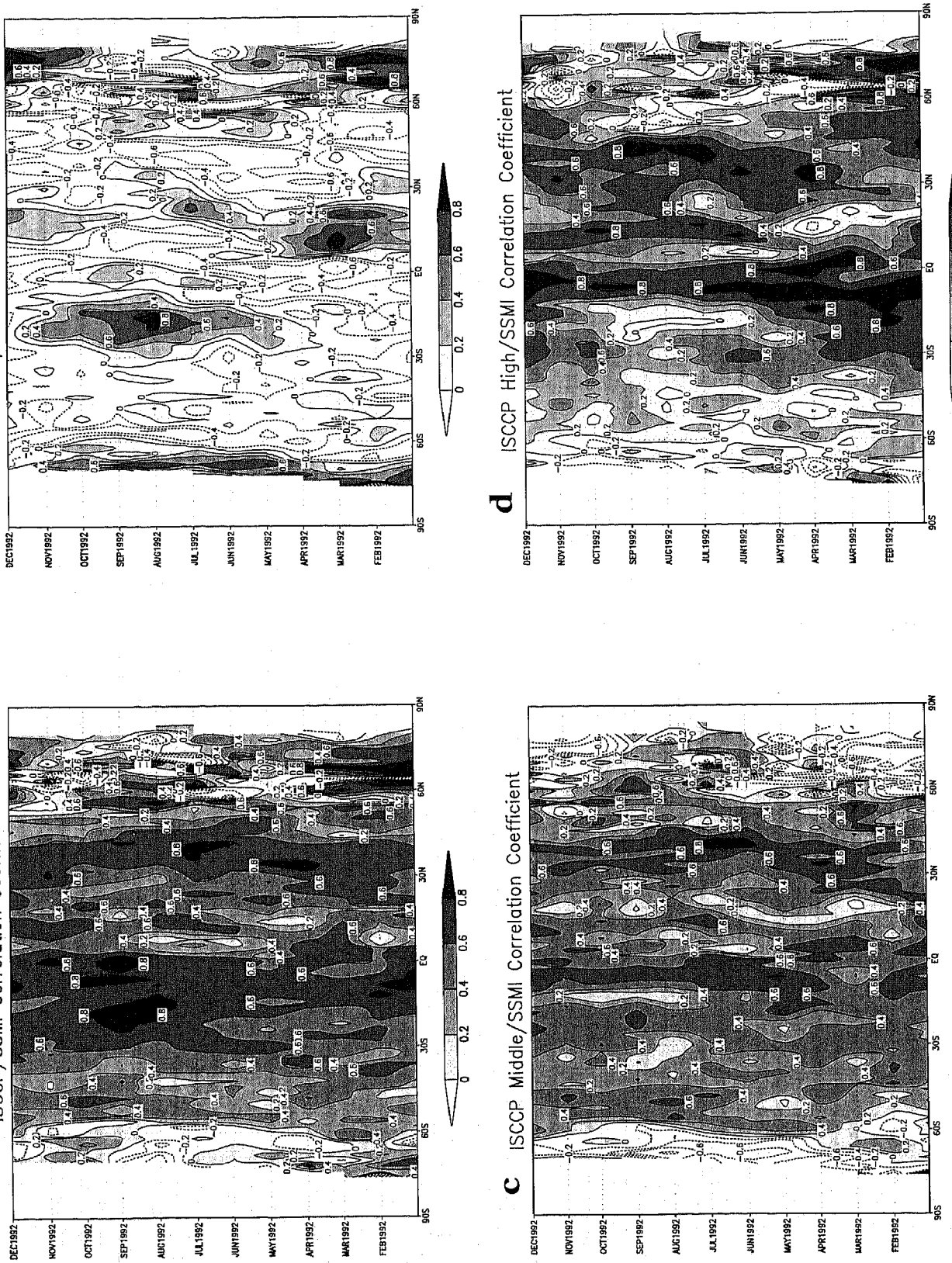

Figure 10. (a-d) Correlation coefficient (R) between monthly mean ISCCP clouds and SSM/I CLW, for the total, low-, middle-, and high-level cloudiness, respectively. Positive values are shaded.

Figure 3], employing a diagnostic parameterization for cloud liquid water which was incorporated in the NCAR Community Climate Model (CCM2). Our extreme values are however somewhat higher than those by *Hack* [1998], but this might be at least partly expected due to the deficiencies of the CCM2 which were mentioned by *Hack* [1998]. In general, the CLW content over the subtropical latitudes, on which we are focusing, is extremely low in both hemispheres. The extreme minimum over the Sahara (below 2 mg cm^{-2}) should be noted in comparison to the high values in the equatorial area and along the extratropical storm tracks. It is interesting to note that as may be expected, the southwest of the United States is much drier in liquid water phase as compared to the southeast (a factor of more than 2-2.5). These and other features look quite reasonable, and some can be traced back to the ISCCP cloudiness variations.

The annual divergence of the CLW fluxes, based on monthly mean winds, is presented in Plate 1b in units of millimeter per day, along with vertically integrated horizontal CLW flux vectors. Positive divergence is depicted in red shadings, and negative divergence (or positive convergence) in blue shadings, as shown on the color bar to the right. Values of CLW divergence are of the order of 0.1 mm/d or less, generally smaller than typical values of vertically integrated moisture divergence. It is interesting to note the following exceptionally higher values. Over the eastern coasts of both the United States and Asia, in the vicinity of the Gulf Stream and Kuroshio currents, respectively, significant positive divergence of CLW fluxes exist, as was earlier conjectured by *Peixoto* [1973]. The CLW flux vectors indicate that clouds are being advected to the east of these regions. Another distinct region of positive divergence is over the Arabian-Iraqi desert at 30°N, 45°E (Plate 1c) and is discussed in section 4.

3.4. CLW and Cloud Types

Applying method **B**, the multiple linear regression (equation (8)) enables the division of the CLW into three constituents from low-, middle-, and high-level clouds. Employing the minimum sum-of-squares method for the data over ocean (64,645 points) yields the global α, β, and γ constants (in millimeter units); hence

$$w = 0.127 \cdot c_{\text{low}} + 0.162 \cdot c_{\text{mid}} + 0.179 \cdot c_{\text{high}}, \qquad (9)$$

where the standard error of the coefficients is 0.002 mm, the coefficient of determination $R^2 = 0.579$, and the statistic $F = 36,952$. With this high F-observed statistic the formula is significant at the 99% level.

It is interesting to note that the scaling constants α, β, and γ increase with the level of the clouds; that is, the scaling factor for the high-level clouds γ is larger than β for the middle level, which is larger than α for the low level. As discussed before, this must be because the ISCCP cloud level is defined only by the cloud-top pressure, and therefore deep convection clouds are classified as high clouds, while low clouds include mostly stratus or other shallow clouds. The R^2 value is as high as the $R^2 = 0.584$ obtained with method **A**.

Figure 11 shows the resulting 1992 annual mean CLW global distribution. In spite of the simplicity of this method, using only three constants, the features are remarkably similar to both the original observations over ocean (Figure 9) and the results from method **A** (Plate 1a). However, unlike method **A**, method **B** enables the division of the vertically mean CLW into its three constituents according to low-, middle-, and high-level clouds and also allows the calculation of the corresponding CLW fluxes separately employing the corresponding winds at the pertinent altitude.

Plates 2a-2d show the resulting CLW fluxes and divergence for the vertically integrated, low, middle, and high clouds, respectively. Plate 2a is the sum of all three levels (notice the slightly different scales in the color shading bars). The mean winds from GEOS-1/DAS at sigma levels 0.8741, 0.7345, and 0.5005 were used for the low, middle, and high clouds, respectively. The vertically integrated Plate 2a is different than Plate 1b (based on method **A**) in the following aspects: Fluxes and divergences are in general smaller than in Plate 1b, because of the use of lower-level winds and different cloud levels which sometimes have anticorrelated contributions. In particular, divergence occurs over the west coasts of North and South America, coupled with convergence in land, while in Plate 1b, it is different. The relatively large divergences over the east coast of both North America and Asia in Plate 1b are much weaker in Plate 2a. The divergence in the vicinity of the Arabian-Iraqi desert is still prominent as well as the pronounced divergence in the vicinity of the Himalayas. These differences demonstrate the strong impact of vertical wind shear on the CLW flux-divergence field. Similarly, *Wang and Paegle* [1996] indicated that the noise/signal ratio of moisture budgets may be improved more rapidly by providing better wind data than by providing better moisture data.

A noted feature in the low-cloud component (Plate 2b) is the divergence of the stratus clouds off the west coasts of the continents due to easterly winds. The low-cloud contribution to the vertically integrated CLW flux divergence is generally smaller in comparison with the middle- and high-cloud contributions, because the smaller CLW content in the low clouds, i.e., the smaller scaling factor in equation (9), and the weaker winds. The middle- and high-cloud components (Plates 2c-2d, respectively) reveal the transport of clouds from the west coasts of the continents into land by the midlatitude westerly winds and the opposite transport of clouds from land into ocean by the easterlies of the ITCZ.

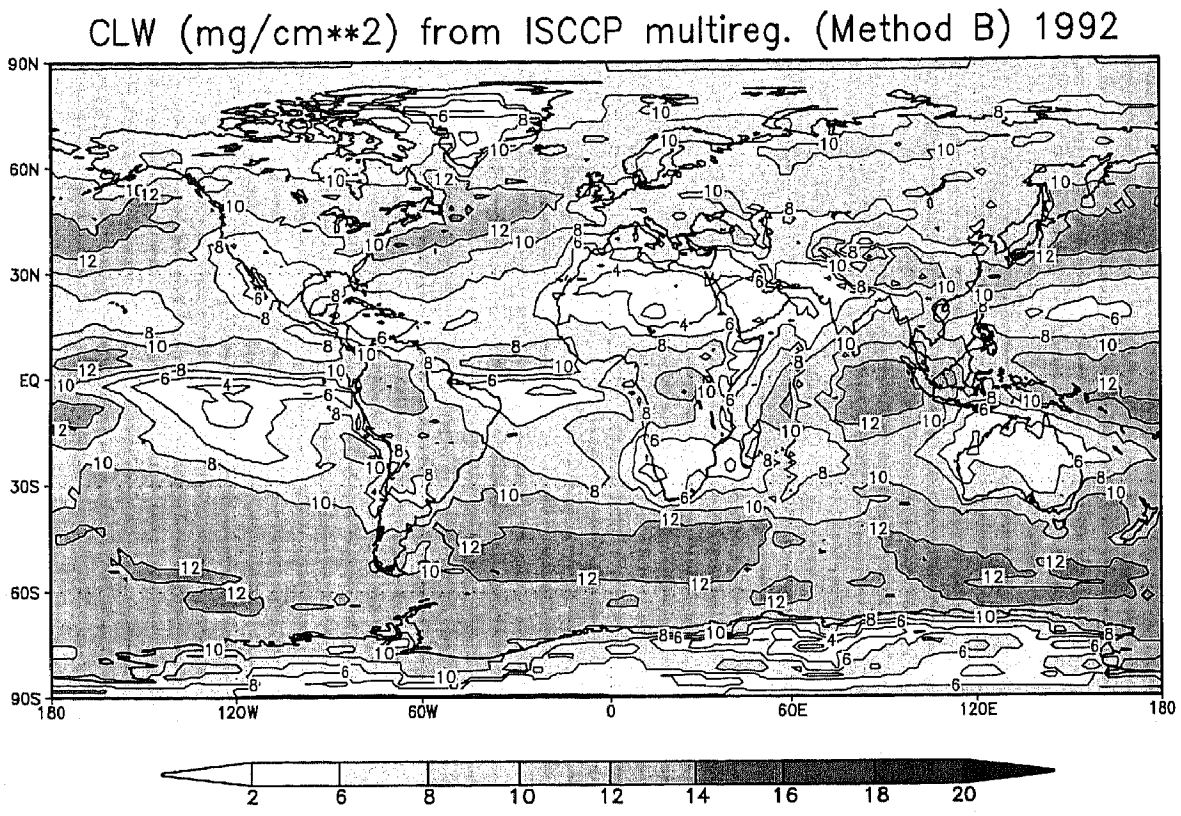

Figure 11. Same as in Figure 9 but calculated by multilinear regression from ISCCP cloudiness, using method B, i.e., equation (8).

4. CLW and Subtropical Moisture Paradoxes

4.1. Arabian Net Sink Paradox

The study of the moisture budget, based on the NASA GEOS-1/DAS reanalysis data set (section 2), confirmed our earlier finding by AS of a paradoxical net moisture sink over the Arabian Peninsula. In this section we investigate whether the explicit CLW fluxes can provide an answer to this paradox. Plate 1c shows the annual divergence of the CLW fluxes, as in Plate 1b, but focused over the Middle East region. The most distinct features are the divergence bands surrounding the Persian Gulf. In particular, the maximum over the whole region is 0.14 mm/d at the grid point 47.5°E, 28°N west of the Persian Gulf. This point is very close to point A at 45°E, 30°N (Figure 1a) where AS found a maximum of net winter moisture vapor convergence. This high proximity in location supports at least qualitatively the AS hypothesis.

A larger value of 0.32 mm/d is obtained for the CLW flux divergence at the same grid point when using only the December-February winter months (e.g., Figure 13, to be discussed). Even this value, however, is too small in comparison with the maximum moisture convergence value of 109 W m^{-2} (equivalent to 3.81 mm/d) at point A for the same winter months (Figure 1a), or even the smaller recent estimate from GEOS-1/DAS of ~30 W m^{-2} (~1 mm/d, Figure 1b). It is also smaller than the annual vertically integrated IAU(q) in this region (~1 mm/d, Figure 2e). Nevertheless, this quantitative difference may depend strongly on the calibration of the CLW retrievals, and on the limitations of the regression method as outlined in section 3.1. In particular, and since ice is an important contributor to high- and middle-level cloudiness in these subtropical latitudes, it is likely that the neglect of ice effects in the SSM/I retrieval algorithm could result in an underestimation of the CLW values (or more precisely the nonvapor water contents). Also, the CLW algorithm stops when rain is detected [*Wentz*, 1995]. This too might be a reason for the underestimated CLW in rain or even evaporating rain conditions. The evaporating rain, i.e., virga, is a frequent phenomenon over the Saudi-Iraqi desert [*Rosenfeld and Mintz*, 1988]. Another reason for underestimating the CLW is due to the difference between marine clouds and continental clouds. Over ocean, low-level clouds are predominant [*Rossow and Schiffer*, 1991]. Low-level clouds are found here to hold less liquid water. Consequently, since the regression formula was calculated only over ocean, it is expected that the continental clouds might hold larger amounts of CLW than those based on the ocean-regressed formula.

Plates 3a-3d show the CLW fluxes and divergence for the vertically integrated, low, middle, and high clouds,

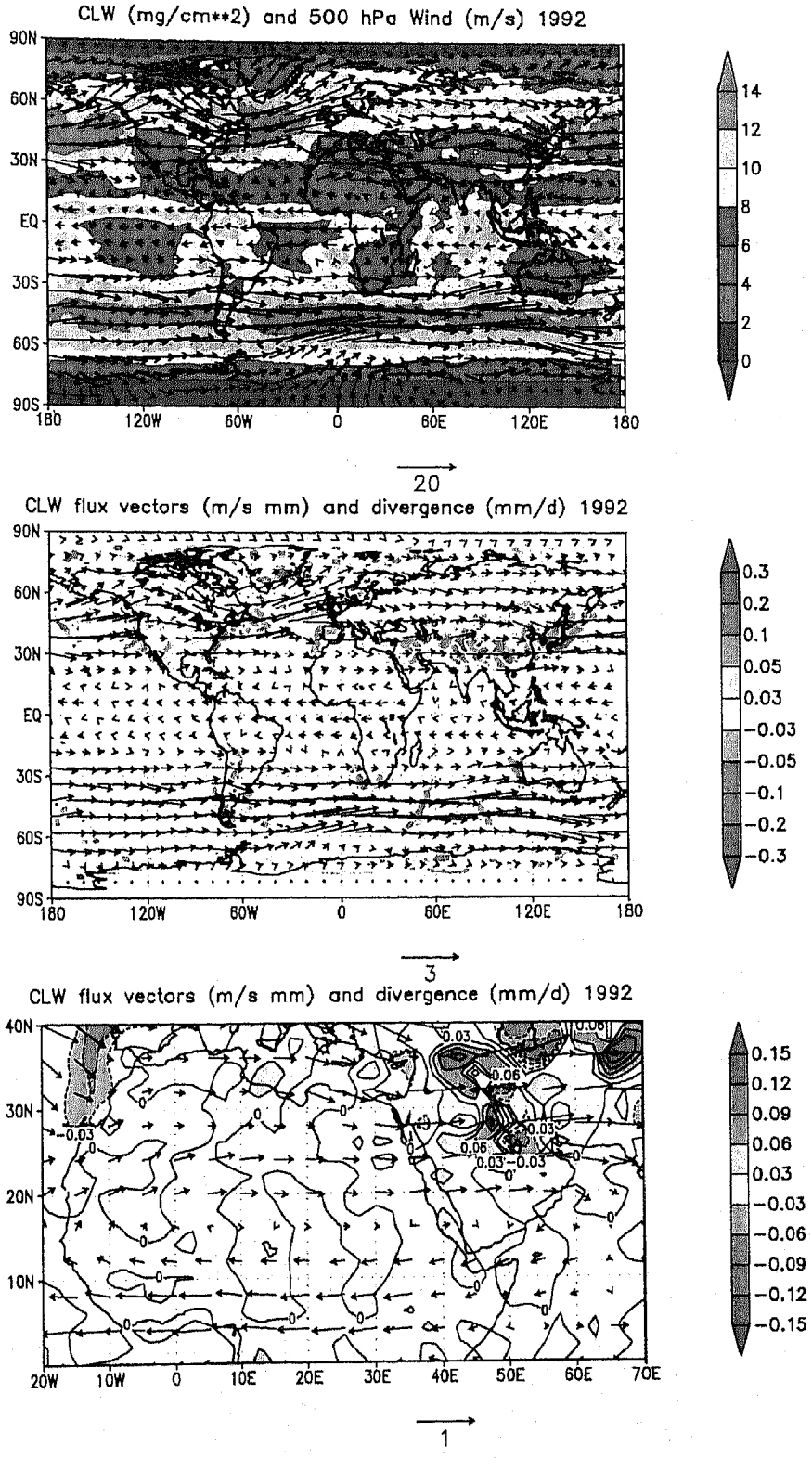

Plate 1. 1992 mean CLW calculated by regression with ISCCP total cloudiness using method **A**, i.e., equation (7): (a) As in Figure 9 but with extension to land. High CLW values are in red and low values in blue, as in the bar at the right. The 500 hPa wind vectors from GEOS-1/DAS, used for flux calculation, are also plotted with a skip of 4 in both latitude and longitude. (b) Resulting CLW flux vectors and divergence of the CLW flux (mm/d); positive values above 0.03 mm/d are depicted in gradual red shadings and negative values below -0.03 mm/d in blue, as in the color bar at the right. (c) As in Plate 1b but focused on the Middle East and the Mediterranean regions; with contours in intervals of 0.03 mm/d and vectors with a skip of 2. Notice the enhanced color shadings.

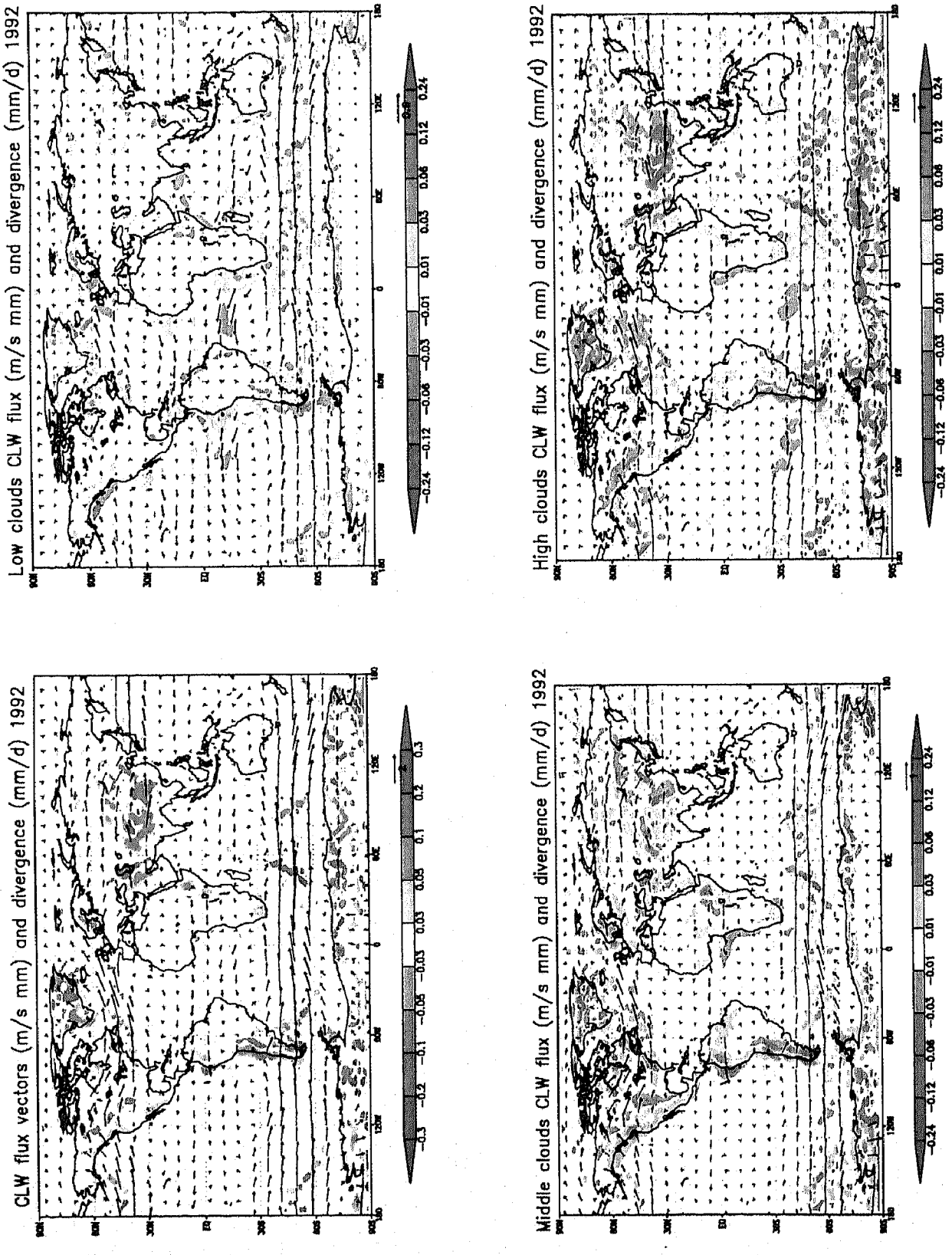

Plate 2. (a-d) CLW fluxes and divergence, as in Plate 1b but calculated by using method **B** for the vertically integrated, low, middle, and high clouds. The vertically integrated Plate 2a is the sum of all three levels. Notice the different scales in the color shading bars.

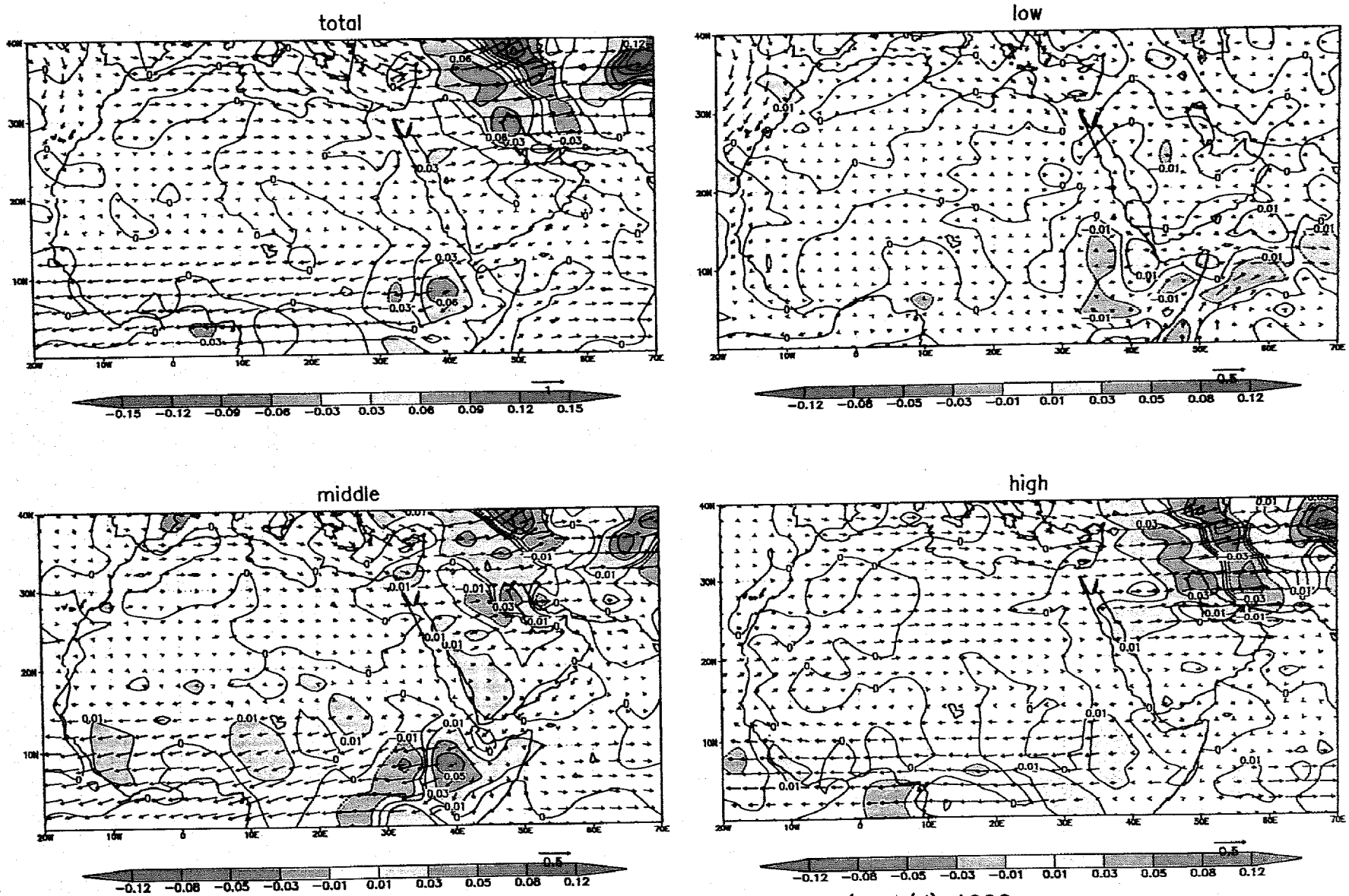

Plate 3. (a-d) Same as Plates 2a-2d but focused on the Middle East and the Mediterranean regions.

respectively, as in Plate 2, but focused on the Middle East region. The positive vertically integrated divergence band (Plate 3a) is somewhat smaller in value than in Plate 1c and is shifted to the northeast. The location corresponds better with the maximal moisture convergence band over the Zagros Mountains stretching to the northwest of the Persian Gulf (~45°E, 35°N, in Figure 2a). It is clear that the CLW total divergence is composed mainly of middle- and high-level clouds (Plates 3c-3d, respectively) with a small negative contribution to the total divergence due to convergence of low-level clouds over the Arabian Peninsula (Plate 3b). This vertical distribution agrees well with the analysis of the vertical profiles of the moisture terms described in section 2d, as well as with the surface cloud observations analyzed by AS.

The CLW calculations, so far, were only for 1992 for which CLW data were available. Figures 12a-12c show the 1985-1990 multiannual mean ISCCP cloud flux divergence for low-, middle-, and high-level clouds, using the GEOS-1/DAS monthly mean winds at 850, 700, and 500 hPa, respectively. The divergence is given in units of %/6 h. On the basis of the regression formula for 1992 (equation (9)), this can be converted to CLW flux divergence by multiplying by $0.5088, 0.6484, 0.6804 \times 10^{-2}$ mm/d for the low, middle, and high clouds. Negative values, i.e., convergence, are shaded. The features over the Arabian Peninsula are similar to the 1992 Plate 3, with low-level cloud convergence topped by middle- and high-level divergence. Conversely, divergence of low-cloud flux topped by middle-cloud convergence occurs near the Persian Gulf (47.5°E, 28°N). This latter relationship accords well with the descending branch of the convection cell over the Arabian peninsula studied in section 2.

4.2. Saharan Net Source Paradox

Another subtropical moisture paradox is the net source over the North African Sahara Desert, found by *Starr and Peixoto* [1958], *Peixoto* [1960], and further investigated by *Shay-El and Alpert* [1991], AS, *Vitart et al.* [1996], and recently by *Shay-El et al.* [1999]. One explanation for this apparent domination of evaporation over precipitation, as suggested by *Peixoto* [1960], is the supply of water by surface and underground flow from less arid areas. However, vertical profiles of moisture budget terms, calculated by *Shay-El and Alpert* [1991], indicate that the Saharan net source originates mainly at levels above 850 hPa and is probably associated with evaporating clouds.

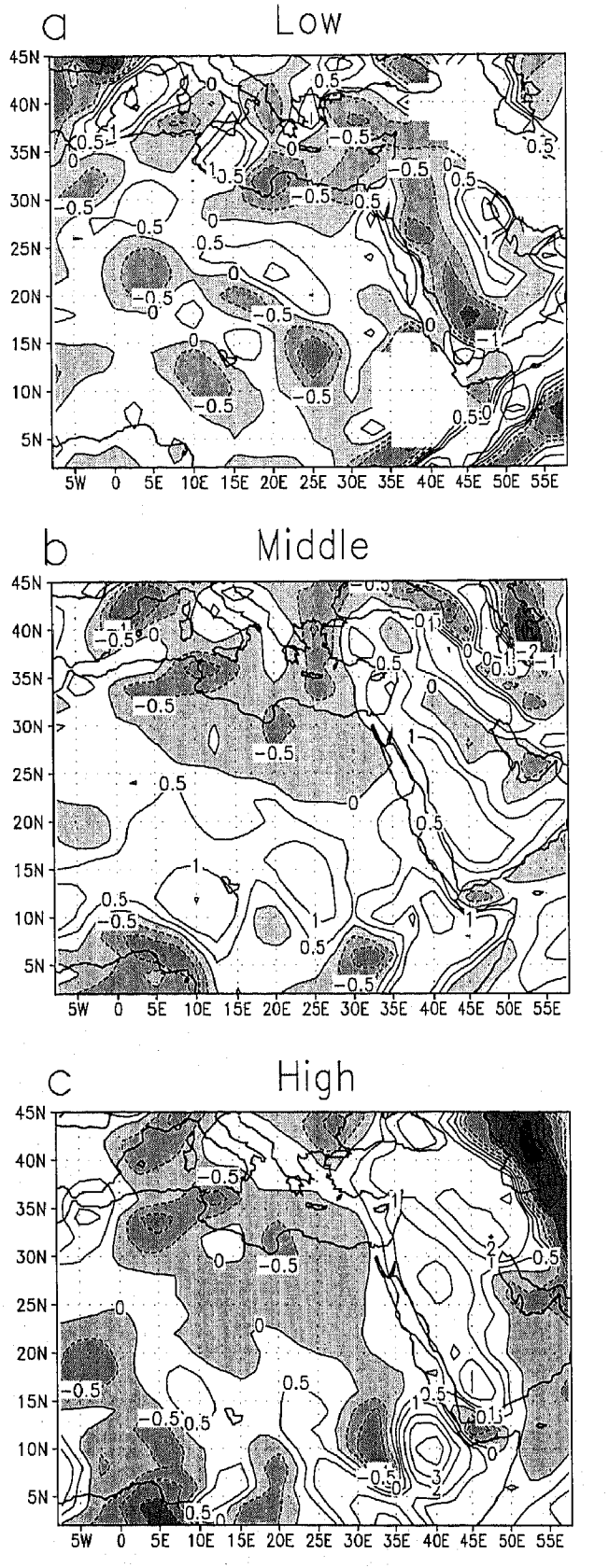

Figure 12. (a-c) 1985-1990 multiannual mean ISCCP cloud flux divergence (in %/6 h) for low-, middle-, and high-level clouds, using the GEOS-1/DAS monthly mean winds at 850, 700, and 500 hPa. Negative values are shaded.

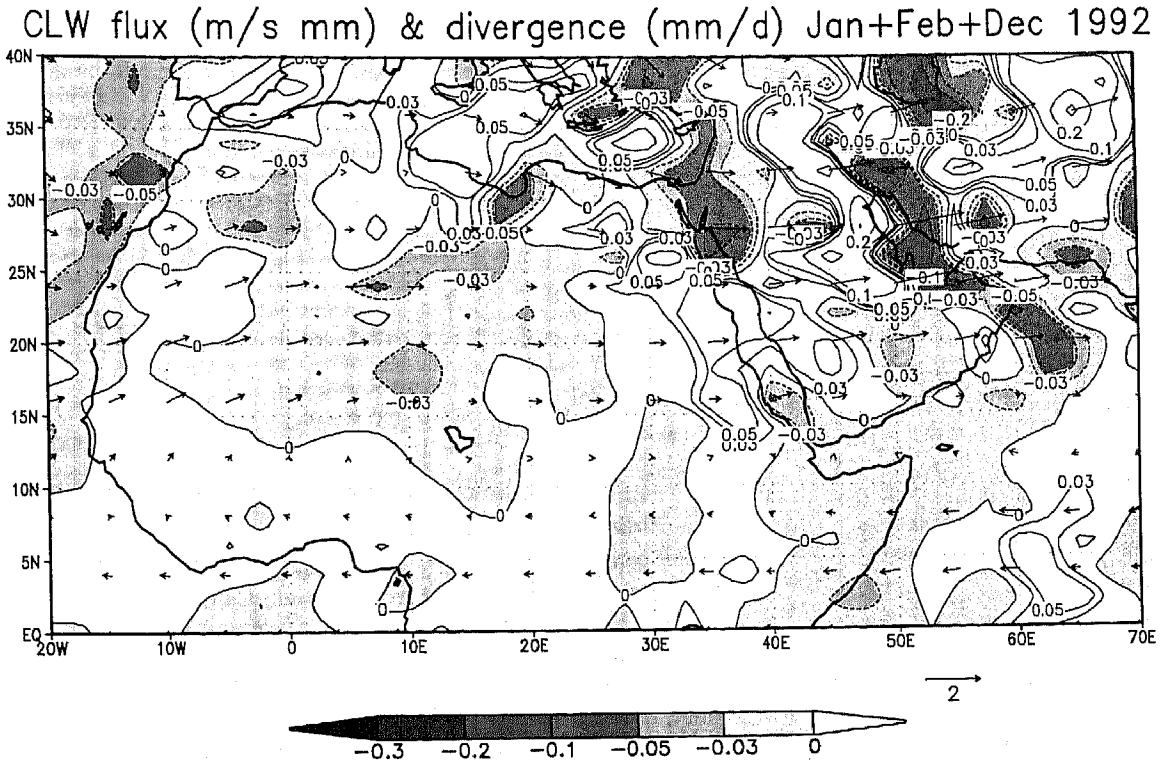

Figure 13. Same as Plate 1c but for the 1992 January-February-December months only. Contour levels are $0, \pm 0.03, \pm 0.05, \pm 0.1, \pm 0.2, \pm 0.3$ mm/d. Negative values are shaded.

Figure 13 shows large regions where convergence of CLW flux takes place during winter 1992 over the northeastern Sahara desert of up to 0.06 mm/d (shaded areas). This flux is mainly associated with clouds from the Mediterranean. CLW converges also over the southwestern Sahara from an Atlantic source. The annual mean values shown in Plate 1c are somewhat reduced due to CLW divergence during summertime, mainly by the easterlies over central Africa.

The locations of the multiannual ISCCP cloudiness convergence regions (shaded in Figures 12a-12c) suggest that middle- and high-level clouds, penetrating from both the Mediterranean and the Atlantic, gradually evaporate in the process of intruding the dry Sahara region. Alternative explanations for the apparent moisture source over the Sahara, such as the diurnal variations of the sea-land breeze, which might pump water vapor into the continent, are currently being investigated. It must also be mentioned that the net source in the assimilated data sets might be due to excessive parameterized evaporation near the coasts of the continent (see further discussion by *Shay-El et al.* [1999]).

5. Discussion and Conclusions

The main purpose of this work was to obtain a preliminary quantitative estimate of the magnitude of the cloud liquid water term in the moisture budget equation which is normally neglected. In general, $\nabla \cdot \overline{\mathbf{Q}}$ is of the order of several millimeters per day when monthly or annual averages are calculated; actual daily values, however, can reach 10^2 mm/d or higher with values comparable to that of the precipitation. The divergence of the water fluxes, $\nabla \cdot \overline{\mathbf{Q}_c}$, however, was found to be smaller by 2 orders of magnitude (or about 300). The aforementioned factor of about 300 relates to the fact that monthly averages of integrated vapor flux $\mathbf{Q}$ are larger by this proportion as compared to integrated liquid water flux $\mathbf{Q}_c$. For instance, integrated water vapor over the intertropical convergence zone for January reaches a maximum of about 6 g/cm^2 (according to GEOS-1/DAS estimates), while the SSM/I-derived integrated CLW at the same region reaches a maximum of only about 20 mg/cm^2. For instantaneous values, however, this proportion drops dramatically to a factor of only 3-4. For instance, in a cumulus maritime cloud simulation with 100 Cloud Condensation Nuclei (CCN) and cloud tops of 4-5 km, the vapor to water ratio increases up to 32:9 g/cm^2 (Z. Levin, personal communication, 1997). It seems therefore that the potential to extract considerable moisture from divergence of cloud liquid water indeed exists, on the condition that the flow and dynamics over specific regions consistently support a certain direction for converting water into vapor or vice versa. This is in fact a common feature for coastal regions or prominent topographical areas.

For our preliminary evaluation the SSM/I CLW retrievals over oceans were combined with ISCCP cloudiness to calculate the cloud liquid water over the continents, using linear regression methods. The coefficient of determination R^2 for 1992 was as high as 0.58. The CLW content was found to be larger for ISCCP high-level clouds than for middle-level clouds, and the smallest for low-level clouds. This is associated with the type of definition of clouds based on a cloud-top-pressure criterion. The globally derived annual mean CLW field seems to correspond well to cloud observations and to model estimations. Divergence of CLW fluxes was computed with the aid of the NASA reanalyzed GEOS-1/DAS monthly mean winds for 1992. It was found that over the eastern coasts of both North America and Asia, in the vicinity of the Gulf Stream and Kuroshio currents, respectively, significant positive divergence of CLW fluxes was prominent, as earlier conjectured by *Peixoto* [1973]. The CLW flux vectors suggest that clouds are being consistently advected to the east of these regions. Middle and high clouds are advected also from the west coast of continents into land by the midlatitude westerly winds. These results, however, are strongly influenced by the wind field.

The net moisture sink found over the Arabia-Iraqi desert during winter was earlier investigated using the ECMWF-analyzed data set for 6 years. Reexamination with the NASA GEOS-1/DAS reanalysis data confirmed this finding. The vertical profiles of the incremental analysis updates, i.e., IAU(q), and of the moist parameterizations, indicate that the sink is associated with middle- and high-level clouds in this region. In both the Arabian-Iraqi desert and over the Sahara, signs for the divergence of cloudiness fluxes were found in the opposite sign to the vertically integrated horizontal moisture flux divergence, thus explaining at least qualitatively the net sink and source in both regions. However, the magnitude of the CLW flux divergence as calculated here is too small when compared with the net moisture source/sink. This might be partly due to underestimation of the CLW content over land. On the other hand, the option that there might be biases in the estimation of the dynamical term of the moisture balance equation, i.e., $\nabla \cdot \overline{\mathbf{Q}}$, based on data assimilation system, cannot be ruled out [see *Shay-El et al.*, 1999].

Our results suggest that over specific regions where flow and dynamics act in a consistent manner, such as in coastal regions, the role of the liquid water divergence in the climatic moisture budget may become significant. This seems to be particularly important in regions where precipitation and evaporation are relatively small, such as over dry subtropical deserts, and in mesoscale active regions where clouds may preferably generate or dissipate in a systematic manner.

Acknowledgments. This study was supported by the US-Israel Binational Science Foundation grant 92-00275. This work was partly performed while the first author (PA) held a National Research Council–NASA/GSFC Research Associateship. Thanks are extended for the valuable discussions with A. Oort and the late J. P. Peixoto (to whom we dedicate this paper) during a seminar given by P. Alpert in GFDL in March 1996. We wish to thank Z. Levin who provided us with cumulus simulation results and to A. Khain for estimations of liquid water content in various clouds. Special gratitude goes to C. Pabon for useful discussions and advice in scaling of the clouds contribution. D. Slozberg is acknowledged for reviewing the English grammar. A. da Silva is supported by the EOS Interdisciplinary Science Program and by the NASA Research and Applications Program. Computer resources and funding were provided by the EOS Project through the Scientific Computational Facility of the Data Assimilation Office.

References

Alpert, P., and Y. Shay-El, The paradox of the winter net moisture sink over the Arabian-Iraqi desert, *Ann. Geophys., 11,* 190–194, 1993.

Doty, B., The Grid Analysis and Display System—GrADS, 148 pp., http://grads.iges.org/grads/head.html, Cent. for Ocean-Land-Atmos. Stud., Calverton, Md., 1995.

Ferraro, R. R., F. Weng, N. C. Grody, and A. Basist, An eight year (1987-1994) time series of rainfall, clouds, water vapor, snow cover and sea ice derived from SSM/I measurements, *Bull. Am. Meteorol. Soc., 77,* 891–905, 1996.

Gibson, J. K., A. Hernandez, P. Kallberg, A. Nomura, E. Serrano, and S. Uppala, The ECMWF re-analysis project, in *Preprints, Tenth Conference on NWP,* pp. 288–291, Am. Meteorol. Soc., Boston, Mass., 1994.

Greenwald, T. J., G. L. Stephens, S. A. Christopher, and T. H. Vonder Haar, Observations of the global characteristics and regional radiative effects of marine cloud liquid water, *J. Clim., 8,* 2928–2946, 1995.

Hack, J. J., Sensitivity of the simulated climate to a diagnostic formulation for cloud liquid water. *J. Clim., 11,* 1497–1515, 1998.

Kalnay, E., et al., The NCEP/NCAR 40-Year Reanalysis Project, *Bull. Am. Meteorol. Soc., 77,* 437–471, 1996.

Min, W., and S. D. Schubert, The climate signal in regional moisture fluxes: A comparison of three global data assimilation products. *J. Clim., 10,* 2623–2642, 1997a.

Min, W., and S. Schubert, Interannual Variability and Potential Predictability in Reanalysis Products, *NASA Tech. Memo. 104606,* vol. 13, Goddard Space Flight Cent., Greenbelt, Md., 1997b.

Peixoto, J. P., On the global water vapor balance and the hydrological cycle, in *Tropical Meteorology in Africa,* pp. 232–243, Munitalp Found., Nairobi, 1960.

Peixoto, J. P., Atmospheric vapor flux computations for hydrological purposes, *WMO Publ. 357,* 83 pp., World Meteorol. Organ., Geneva, 1973.

Peixoto, J. P., and A. H. Oort, *Physics of Climate,* 520 pp., Am. Inst. of Phys., New York, 1992.

Rosenfeld, D., and Y. Mintz, Evaporation of rain falling from convective clouds as derived from radar measurements, *J. Appl. Meteorol., 27,* 209–215, 1988.

Rossow, W. B., and R. A. Schiffer, ISCCP cloud data products, *Bull. Am. Meteorol. Soc., 72,* 2-20, 1991.

Rossow, W. B., A. W. Walker, and L. C. Gardner, Comparison of ISCCP and other cloud amounts, *J. Clim., 6,* 2394–2418, 1993.

Rossow, W. B., A. W. Walker, D. E. Beuschel, and M. D. Roiter, International Satellite Cloud Climatology Project (ISCCP) documentation of new cloud data sets, *WMO/TD-737,* 115 pp., World Meteorol. Organ., Geneva, 1996.

Schubert, S., R. Rood, and J. Pfaendtner, An assimilated data set for Earth Sciences applications, *Bull. Am. Meteorol. Soc., 74,* 2331–2342, 1993.

Schubert, S. D., H. M. Helfand, C.-Y. Wu, and W Min, Subseasonal variations in warm-season moisture transport and precipitation over the central and eastern United States, *J. Clim., 11,* 2530–2555, 1998.

Schubert, S., C.-K. Park, C.-Y. Wu, W. Higgins, Y. Kondratyeva, A. Molod, L. Takacs, M. Seablom, and R. Rood, A multiyear assimilation with the GEOS-1 system: Overview and results, *NASA Tech. Memo. 104606,* vol. 6, Goddard Space Flight Cent., Greenbelt, Md., 1995.

Shay-El, Y., and P. Alpert, A diagnostic study of winter diabatic heating in the Mediterranean in relation to cyclones, *Q. J. R. Meteorol. Soc., 117,* 715–747, 1991.

Shay-El, Y., P. Alpert, and A. da Silva, Reassessment of the moisture source over the Sahara Desert based on NASA reanalysis, *J. Geophys. Res., 104,* 2015–2030, 1999.

Starr, V. P., and J. P. Peixoto, On the global balance of water vapor and the hydrology of deserts, *Tellus, 10,* 189–194, 1958.

Sud, Y. C., and A. Molod, The roles of dry convection, cloud-radiation feedback processes and the influence of recent improvements in the parameterization of convection in the GLA GCM, *Mon. Weather Rev., 116,* 2366–2387, 1988.

Takacs, L. L., A. Molod, and T. Wang, Documentation of the Goddard Earth Observing System (GEOS) General Circulation Model–Version 1, *NASA Tech. Memo. 104606,* vol. 1, Goddard Space Flight Cent., Greenbelt, Md., 1994.

Trenberth, K. E., and C. J. Guillemot, Evaluation of the atmospheric moisture and hydrological cycle in the NCEP/NCAR reanalyses, *Clim. Dyn., 14,* 213–231, 1998.

Vitart, F., A. H. Oort, and K. Mo, New results on the hydrology of the North African desert, based on the NMC reanalysis, in *Proceedings of the 20th Climate Diagnostics Workshop,* pp. 191–194, U.S. Dep. of Comm./NOAA/NWS, Washington, D. C., 1996.

Wang, M., and J. Paegle, Impact of analysis uncertainty upon regional atmosphere moisture flux, *J. Geophys. Res., 101,* 7291–7303, 1996.

Wentz, F., A well calibrated ocean algorithm for SSM/I, *RSS Tech. Rep. 101395,* 34 pp., Remote Sens. Syst., Santa Rosa, Calif., 1995.

P. Alpert and Y. Shay-El, Dept. of Geophysics and Planetary Sciences, Tel-Aviv University, Tel-Aviv 69978, Israel. (e-mail: yuval@cyclone.tau.ac.il; pinhas@cyclone.tau.ac.il)

A. da Silva, Data Assimilation Office, code 910.3, NASA/GSFC, Greenbelt, MD 20071.
(e-mail: dasilva@niteroi.gsfc.nasa.gov)

(Received June 18, 1999; revised November 23, 1999; accepted November 29, 1999.)